

Improvement of Cell Performance in Low-Pt-Loading Cathode
Catalyst Layers Prepared by the Electrospray Method for Polymer
Electrolyte Fuel Cells (PEFCs)

A Doctoral Thesis

Presented to the

Interdisciplinary Graduate School of Medicine and Engineering

University of Yamanashi

March 2017

Kento Takahashi

Contents

Chapter 1 General Introduction

1.1 Background.....	- 1 -
1.2 Polymer electrolyte fuel cells (PEFCs).....	- 2 -
1.3 Parameters for PEFC performance	- 5 -
1.4 Current status for the improvement of PEFCs	- 8 -
1.5 The mechanism of the electrospray (ES) method	- 9 -
1.6 Objective of Research.....	- 11 -
1.7 References.....	- 12 -

Chapter 2 Mode Variation of the ES Method with Pt/GCB or Pt/Ta-SnO₂

2.1 Introduction.....	- 15 -
2.2 Experimental.....	- 15 -
2.2.1 Preparation of the catalyst ink with Pt/GCB	- 15 -
2.2.2 Preparation of the catalyst ink with Pt/Ta-SnO ₂	- 16 -
2.2.3 Setting parameters of the ES method.....	- 17 -
2.3 Result and discussion.....	- 17 -
2.3.1 The mode changes of ES method with Pt/GCB	- 17 -
2.3.2 Mode changes of ES method with Pt/Ta-SnO ₂	- 21 -
2.4 Conclusions.....	- 25 -

2.5 References.....	- 26 -
---------------------	--------

Chapter 3 Improvement of Cell Performance in Low-Pt-Loading Cathode CLs with Pt/GCB

Prepared by the ES method.

3.1 Introduction.....	- 27 -
-----------------------	--------

3.2 Experimental.....	- 28 -
-----------------------	--------

3.2.1 Preparation of the catalyst ink.....	- 28 -
--	--------

3.2.2 ES method.....	- 28 -
----------------------	--------

3.2.3 Pulse-swirl-spray method.....	- 29 -
-------------------------------------	--------

3.2.3 Preparation and evaluation of the CLs fabricated by PSS or ES methods.....	- 31 -
--	--------

3.2.4 Evaluation of fuel cell performances.....	- 32 -
---	--------

3.3 Result and discussion.....	- 33 -
--------------------------------	--------

3.3.1 Construction of CLs.....	- 33 -
--------------------------------	--------

3.3.2 Microstructure of CLs prepared by PSS and ES methods.....	- 35 -
---	--------

3.3.3 Performance of the cathodes fabricated by the PSS and ES methods.....	- 39 -
---	--------

3.4 Conclusions.....	- 46 -
----------------------	--------

3.5 References.....	- 47 -
---------------------	--------

Chapter 4 Improvement of Cell Performance in Low-Pt-Loading Cathode Catalyst Layers

with Pt/Ta-SnO₂ Prepared by the ES method.

4.1 Introduction.....	- 49 -
-----------------------	--------

4.2 Experimental.....	- 50 -
-----------------------	--------

4.2.1 Preparation of the catalyst ink with Pt/Ta-SnO ₂	- 50 -
---	--------

4.2.2 Preparation of CLs by the pulse-swirl-spray and ES methods.....	- 50 -
4.2.3 Evaluation of the fuel cell performance	- 52 -
4.3 Result and discussion.....	- 53 -
4.3.1 Construction of CLs.....	- 53 -
4.3.2 Morphology comparison of CLs with PSS I/S = 0.7, ES I/S = 0.7 and ES I/S = 0.2.....	- 55 -
4.3.3 Cell performance comparison of PSS I/S = 0.7, ES I/S = 0.7 and ES I/S = 0.2.....	- 62 -
4.4 Conclusions.....	- 70 -
4.5 References.....	- 71 -

Chapter 5 General conclusion

5.1 Conclusions.....	- 73 -
5.2 Future prospects	- 75 -
List of publications	- 76 -
Meeting abstracts	- 76 -
Acknowledgements.....	- 77 -

Chapter 1

General Introduction

1.1 Background

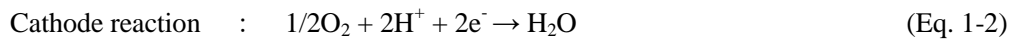
Our life has become comfortable due to a lifestyle based on large-scale production and consumption, which has relied on fossil fuels. The consumption of fossil fuels has increased in the world year by year, and this tendency is expected to continue into the future. However, the amount of fossil fuels is limited, and the enormous amount of fossil fuel consumption has caused serious environmental pollution and global warming. In addition, the accident at the Fukushima nuclear plant in Japan in 2011 shocked the whole world. Thus, many people began to seek safer, more highly efficient, and sustainable energy resources, and researchers around the world have been developing technology on alternative power sources to possibly replace combustion engines and on alternative fuels for solving these crises. Fuel cells have the potential to meet this demand. Fuel cells are electrochemical devices that directly convert chemical energy to electrical energy by means of the electrochemical reaction of oxygen and hydrogen fuel, and produce only water during generation of electricity. Their efficiency is able to reach as high as 60% in electrical energy conversion because of the lack of influence of the Carnot cycle. Fuel cells are able to suppress major pollutants by more than 90% compared with conventional approaches [1]. Fuel cells can mainly be classified into five types by electrolyte: (1) alkaline fuel cells (AFCs), (2) phosphoric acid fuel cells (PAFCs), (3) molten carbonate fuel cells (MCFCs), (4) solid oxide fuel cells (SOFCs) and (5) polymer electrolyte membrane fuel cells (PEMFCs or PEFCs). Among these, the PEFCs have advantages, e.g., short

warm-up time and high specific power. Therefore, investigations have become active recently for cogeneration systems and vehicles. In Japan, commercial cogeneration devices, called ENEFARMS, are being produced by several companies. The total number of device sales reached 10,000 in 2016. Prototype fuel cell vehicles (FCVs) are being produced by several car companies. Toyota Motor Corporation sold the first commercial FCV in the world in 2014, Honda Motor Co., Ltd. also sold commercial FCVs in 2015. Products with PEFCs are anticipated to be developed even further from now on.

1.2 Polymer electrolyte fuel cells (PEFCs)

A schematic diagram of a PEFC is shown in Fig. 1-1. The PEFC consists of a membrane-electrode-assembly (MEA) and two gas diffusion layers (GDLs) sandwiching the MEA.

The electrode reactions and total cell reaction are shown as follows:



The hydrogen enters the anode compartment and diffuses into the gas diffusion layer in the anode catalyst layer (CL). When hydrogen is oxidized at the anode CL, protons and electrons are generated. The protons go through the electrolyte, which is an ion-conductive polymer membrane, and the electrons go through the external circuit. On the other hand, the oxygen enters the cathode compartment and diffuses into the cathode gas diffusion layer into the cathode CL. The oxygen reacts with protons and electrons at the cathode CL to form water. The water is discharged out of the cathode CL through the cathode gas diffusion layer.

The PEFC single cell components are shown in Fig. 1-2. The single cell consists of the MEA, gasket, conductive separators (usually made of graphite or metal), current collectors and endplates. The electron conductive separators are equipped with gas flow channels such as single-, multi-serpentine or parallel channels [2-4]. The MEA and gaskets are sandwiched by two separators and, then, constricted with two endplates. In commercial PEFCs, several tens of single cells are stacked in series in practical usage to obtain useful voltages.

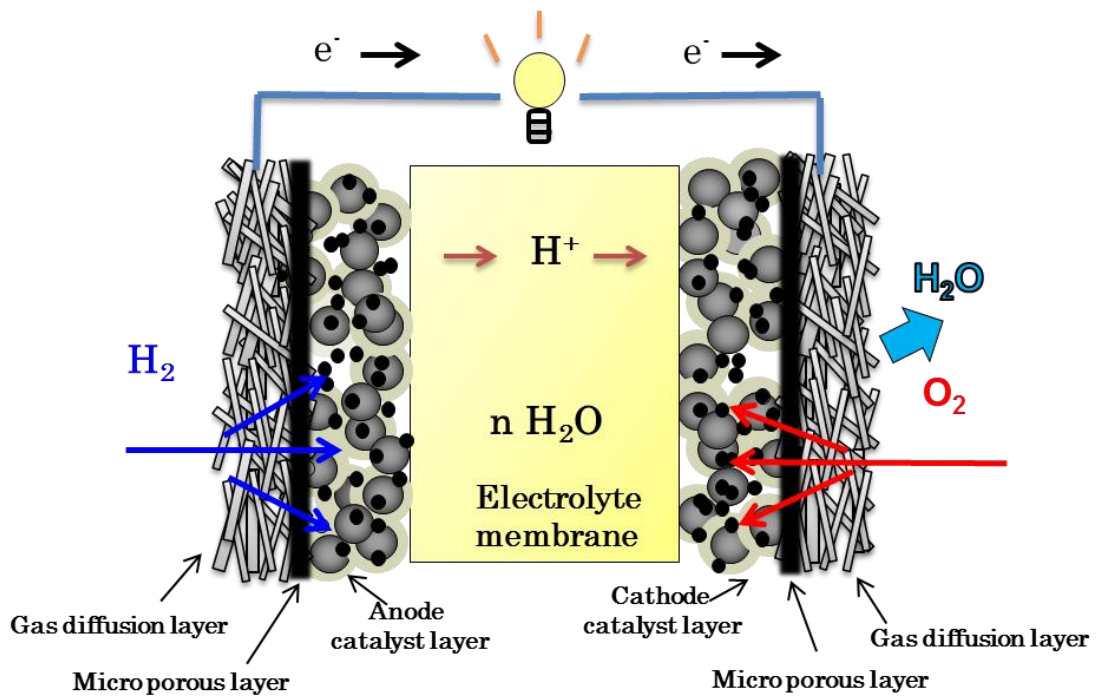


Fig. 1-1 Schematic diagram of an MEA.

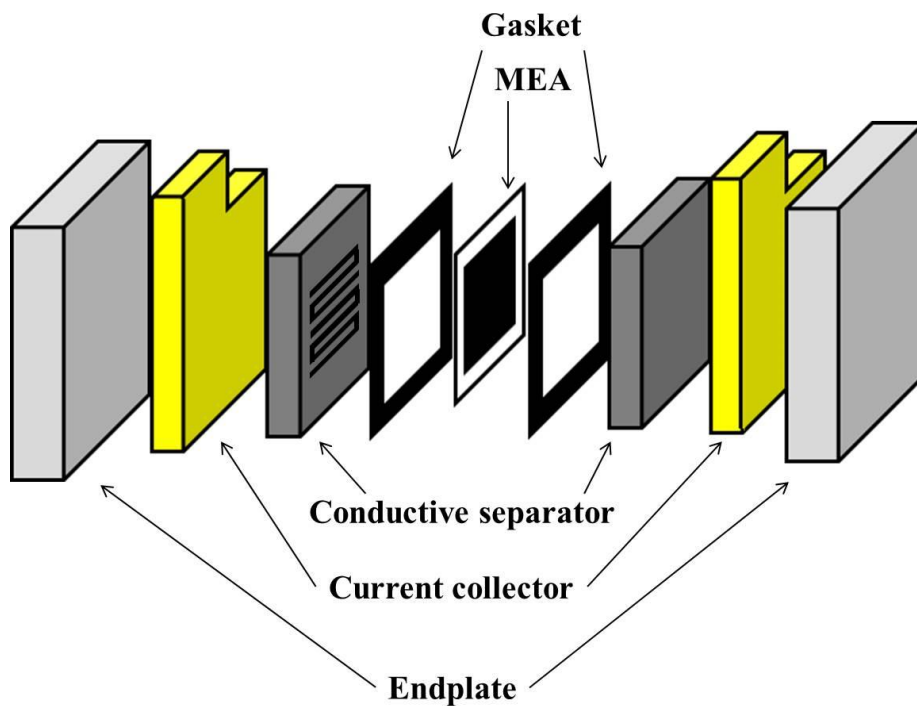


Fig. 1-2 Schematic diagram of a PEFC single cell.

1.3 Parameters for PEFC performance

The cell potential (E) depends on the driven current density (I), and varies as shown in Fig. 1-3. When a current density is not driven (termed open-circuit voltage, OCV), the E achieves a theoretical value of 1.23 V. However, the OCV of a practical cell decreases from 1.23 V, because hydrogen goes through the electrolyte membrane to the cathode (termed a cross-leak of hydrogen), and E becomes nearly 1.0 V. When current density is driven, several types of resistances affect E . The resistances can be separated into an anodic polarization resistance and a cathodic polarization resistance, which are related by Ohm's Law to the anodic overpotential (η^A) and cathodic overpotential (η^c), and the ohmic (IR) loss. The anodic overpotential and cathodic overpotential consist of activation overpotential and concentration overpotential components. The anodic overpotentials are negligible when hydrogen is used as fuel due to fast kinetics of the hydrogen oxidation reaction on the catalyst and the high diffusivity of hydrogen. Therefore, the cathodic activation overpotential (η_{act}^c) and the cathodic concentration overpotential (η_{conc}^c) and IR loss mainly affect the cell performance. The η_{act}^c and η_{conc}^c are generally dominated by catalytic activity for the ORR and mass transport (protons, electron and oxygen) in the cathode, respectively.

The η_{act}^c for the ORR in an acidic environment at the Pt cathode is large, due to the slow kinetics of the ORR. The mass activity (MA) of a catalyst in acid electrolyte solutions for the ORR is defined as follows:

$$MA [A g^{-1}] = j_s [A m^{-2}] \times ECA [m^2 g_{Pt}^{-1}] \quad (\text{Eq. 1-4})$$

where, j_s is the specific activity (current density per active surface area) for the ORR, which has been reported to be enhanced by Pt alloyed with various metals [5-8]. ECA is the electrochemically active surface area, which is calculated from the electrical quantity of charge for hydrogen adsorption from

the cyclic voltammogram. In order to increase the ECA, the catalyst should exist as small particles, and a narrow size distribution and uniform binder distribution on the catalyst are necessary.

The η_{conc}^c generally increases with an insufficient gas supply and is also affected by the dissipation of the product water in the cathode. Therefore, the suppression of the η_{conc}^c can be affected by a hydrophobization treatment of the microporous layer (MPL) [9, 10] and the gas-diffusion layer (GDL) [11, 12], or an increase of the porosity or pore diameter in the GDL [13,14]. In addition, gas flow field designs and operation conditions (cell temperature, gas flow rate and backpressure) have been investigated [9].

The IR loss corresponds to the ohmic resistance of the electrode, electrolytes and separators. When the IR resistance is measured as a high frequency resistance (HFR), the proton transport resistance in the electrolyte membrane is dominant. In order to decrease the membrane resistance, the improvement of proton conductivity and the decrease of membrane thickness are desirable.

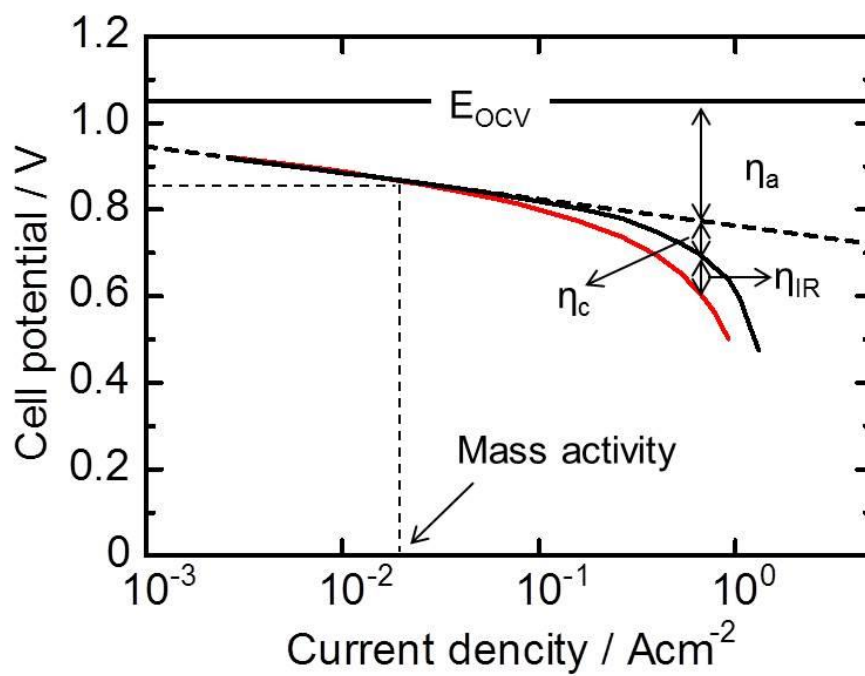


Fig. 1-3 Relationship of activation and concentration overpotentials and *IR* loss in Tafel plot.

1.4 Current status for the improvement of PEFCs

PEFCs have many advantages for electric power generation but also have several problems that need to be solved. One of the problems is the reduction of the PEFC component cost. The catalysts are mainly based on Pt and are used for the hydrogen oxidation reaction on the anode and the oxygen reduction reaction on the cathode. While hydrogen oxidation over platinum is intrinsically very fast, oxygen reduction over platinum is very slow. In fact, the exchange current density of hydrogen oxidation on platinum is almost three orders of magnitude higher than that of oxygen reduction [15,16]. Therefore, many researchers have focused on the development of catalysts for the ORR such as new Pt alloy catalysts, or the control of particle size and Pt-Pt particle distance [17-19]. Our group evaluated the practical utilization of Pt under operating conditions, finding that the effectiveness of Pt was only on the order of 7.5% in air at 65 °C under 0.1 MPa [20]. In order to increase the effectiveness of Pt, we found the relationship of the effectiveness with catalyst layer (CL) thickness and Pt alloy catalyst [21,22]. In particular, the mass activity of the CL was increased by reducing the Pt loading amount in the CL to about 0.05 mg cm⁻². However, it was also found that a new preparation method, which can construct a uniform layer, is necessary to improve the performance of the thin CLs with micrometer-order thickness. The CLs are usually fabricated from a catalyst ink, which includes the Pt catalyst on a support material, an ionomer binder and a dispersant solvent. Then, several researchers have reported the use of inkjet [23], electrospinning [24] and electrospray (ES) [25, 26] methods to fabricate CLs with low Pt loading amounts. In the case of the ES method, micrometer-sized droplets of the catalyst ink can be prepared. The ES method is driven by the electric field between the ejector needle and the substrate, which ejects the ink. The mechanism of the ES method will be explained in the next Section.

1.5 The mechanism of the electrospray (ES) method

A schematic drawing of the ES method is shown in Fig. 1-4a. The device consists of a capillary nozzle (SNA-28G-B, SNA-27G-B, SNA-26G-B, Musashi Engineering, Inc.), usually made from a fine hypodermic needle, and an extractor electrode plate with a single perforation. Usually, the capillary nozzle is connected to a high-voltage supply, while the perforated electrode plate and electrically conductive substrate are grounded. The capillary nozzle is equipped with an ink reservoir containing the catalyst ink which mixed catalyst on support material, ionomer binder and solvent. The capillary nozzle is positioned above the hot substrate, and an electrolyte membrane is placed on the substrate. A high voltage supply (610E, Trek Japan Co., Ltd.) is connected between electrodes, which are fitted into the capillary nozzle (positive), and the substrate (negative). By controlling the electrostatic fields around the nozzle, the ES method can vary the form of the ink ejected from the tip of the nozzle. One of the forms is called a Taylor cone, which is a conically shaped ink meniscus. The mode with formation of a Taylor cone is called the cone-jet mode [27, 28]. In the cone-jet mode, the droplets are electrically charged and are dispersed by electrostatic repulsion. Therefore, the droplets are ejected by electrostatic repulsion with uniform small droplets to micrometer order size. (Fig. 1-4b) [29-31].

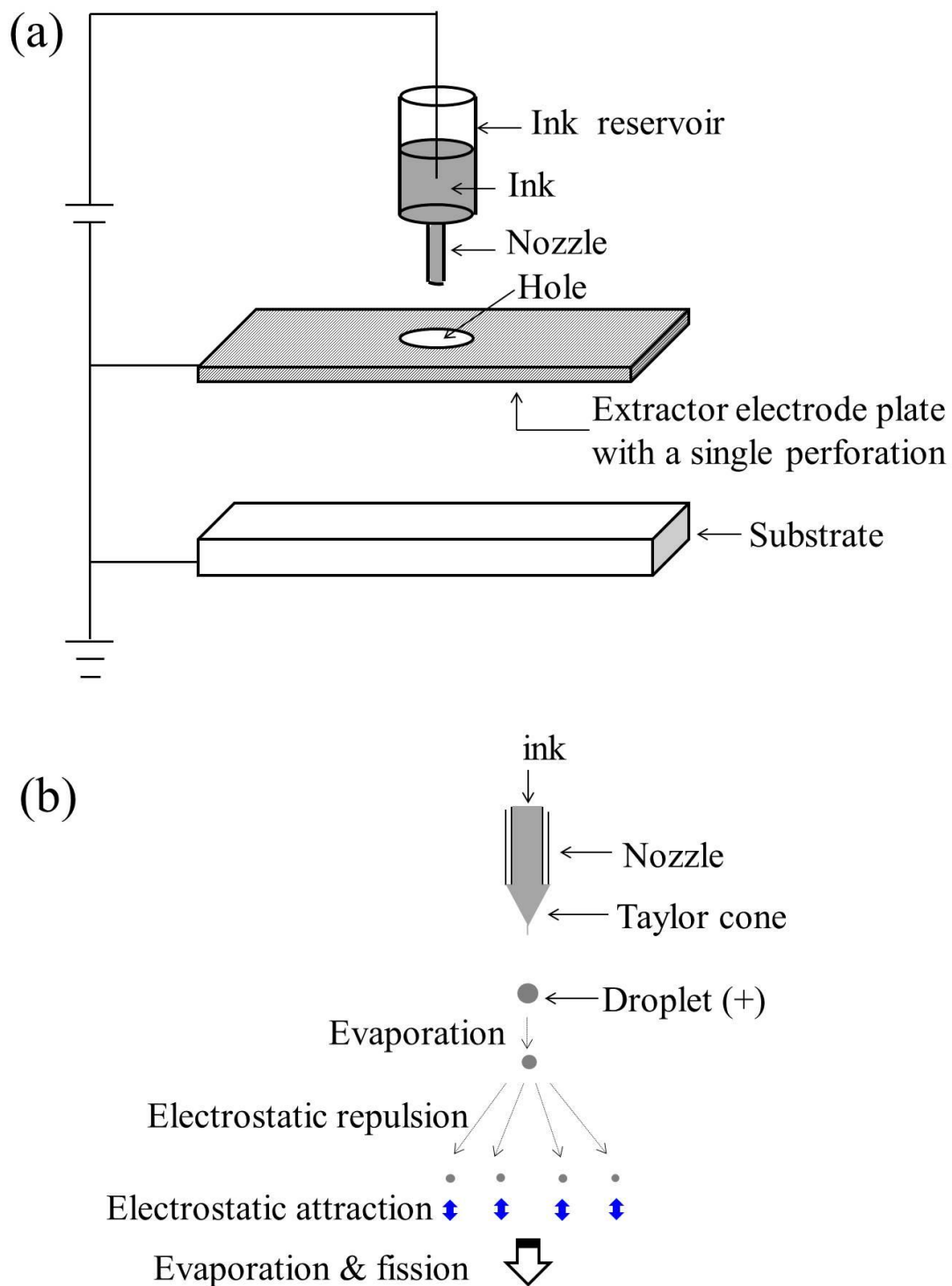


Fig. 1-4 (a) Schematic drawing of electro spray (ES) process; (b) stages of microparticle and nanoparticle production by ES.

1.6 Objective of Research

Several researchers have worked to develop the fabrication method of the low Pt loading CL by the ES method. Chaparro et al. succeeded in the preparation of a CL from a Pt catalyst supported on carbon black by ES and obtained superior performance for a cell with a Pt loading of 0.17 mg cm^{-2} [32]. Benitez et al. showed superior performance compared to that obtained by spray coating [33]. Martin et al. reduced the Pt loading of a CL to 0.012 mg cm^{-2} by the ES method [34]. These results indicated that the ES method has potential to improve the cell performance while reducing the Pt loading amount. However, the fabrication of the low Pt loading CL for the ES method has just begun to be investigated, and the information of the stable ejection of the ink or the analysis of the morphology concerning cell performance are still lacking. Therefore, in order to form CLs by the ES method, the discharge stability of ink using different catalyst support materials were improved, and the relationship between cell performance and morphology of the CL was investigated.

In Chapter 2, the ink with Pt supported on carbon black (CB) or Pt supported on cation-doped metal oxide were found to eject the ink stably. In Chapter 3, I fabricated a low Pt loading amount CL with Pt on CB by the ES method, and by the pulse-swirl-spray (PSS) method. The morphology of the CL for the ES method and PSS method were evaluated, and the cell performances of CLs for the ES method and PSS method were compared. In Chapter 4, low Pt loading CLs by the ES method with the cation-doped metal oxide were prepared. This investigation made use of two inks with different mass ratios of Nafion binder to SnO_2 support (I/S). The cell performances and CL morphology were evaluated. In Chapter 5, the general conclusions and future plan from the results of Chapters 2, 3 and 4 are summarized.

1.7 References

- [1] Papageorgopoulos D. DOE fuel cell technology program overview and introduction to the 2010 fuel cell pre-solicitation workshop in DOE fuel cell pre-solicitation workshop. Department of Energy, Lakewood, Colorado; 2010.
- [2] Kumar, R. G. Reddy, *J. Power Sources*, **114**, 54, 2003
- [3] E. Hontanon, M.J. Escudero, C. Bautista, P.L. Garcia-Ybarra, L. Daza, *J. Power Sources*, **86**, 363, 2000
- [4] X. Li, I. Sabir, *Int. J. Hydrogen Energy*, **30**, 359 , (2005)
- [5] S. Mukerjee, S. Srinivasan, M. P. Soriaga and J. McBreen, *J. Electrochem. Soc.* **142**, 1409, 1995
- [6] T. Toda, H. Igarashi, H. Uchida and M. Watanabe, *J. Electrochem. Soc.* **146**, 3750, 1999
- [7] S. Mukerjee and S. Srinivasan, *J. Electrochem. Soc.*, **357**, 201, 1993
- [8] E. Antolini, R. R. Passos and E. A. Ticianelli, *Electrochem. Acta.* **48**, 263, 2002
- [9] H. Li, Y. Tang, Z. Wang, Z. Shi, S. Wu, D. Song, J. Zhang, K. Fatih, J. Zhang, H. Wang, Z. Liu, R. Abouatallah and A. Mazza, *J. Power Sources*, **178**, 103, (2008)
- [10] S. Park, J.-W. Lee, B. N. Popov, *Int. J. Hydrogen Energy*, **37**, 5850, (2012)
- [11] J. H. Chun, K. T. Park, D. H. Jo, J. Y. Lee, S. G. Kim, S. H. Park, E. S. Lee, J.-Y. Jyoung and S. H. Kim, *J. Hydrogen Energy*, **36**, 8422, (2011)
- [12] S. Hirakata, M. Hara, K. Kakinuma, M. Uchida, D. A. Tryk, H. Uchida and M. Watanabe *Electrochem. Acta.* **120**, 240, (2014)
- [13] H.-S. Chu, C. Yeh and F. Chen, *J. Power Sources*, **123**, 1, (2003)
- [14] S. Hirakata, T. Mochizuki, M. Uchida, H. Uchida and M. Watanabe, *Electrochem. Acta.* **108**,

304, (2013)

- [15] N. M. Markovic, Handbook of Fuel Cells – Fundamentals, Technology and Applications, W. Vielstich, A. Lamm, and H. A. Gasteiger, Editors, Vol. 2, p. 374, John Wiley & Sons Ltd., New York (2003).
- [16] Hamnett, Handbook of Fuel Cells – Fundamentals, Technology and Applications, W. Vielstich, A. Lamm, and H. A. Gasteiger, Editors, Vol. 1, p. 34, John Wiley & Sons Ltd., New York (2003).
- [17] Wang, N. M. Markovic, and V. R. Stamenkovic, *ACS Catal.*, **2**(5), 891, (2012).
- [18] D.A. Cantane, F.E.R. Oliveira, S.F. Santos, F.H.B. Lima, *Appl. Catal. B-Environ.*, **136,137** 351 (2013).
- [19] Z. Liu, M. Shamsuzzoha, E. T. Ada, W. M. Reichert, D. E. Nikles, *J. Power Sources*, **164**, 472 (2007).
- [20] M. Lee, M. Uchida, H. Yano, D. A. Tryk, H. Uchida, and M. Watanabe, *Electrochim. Acta.*, **55**, 8504 (2010).
- [21] M. Lee, M. Uchida, D. A. Tryk, H. Uchida, and M. Watanabe, *Electrochim. Acta.*, **56**, 4783 (2011).
- [22] M. Uchida, Y.-C. Park, K. Kakinuma, H. Yano, D. A. Tryk, T. Kamino, H. Uchida, and M. Watanabe, *Phys. Chem. Chem. Phys.*, **15**, 11236 (2013).
- [23] S. Shukla, K. Domican, K. Karan, S. Bhattacharjee, and M. Secanell, *Electrochim. Acta.*, **156**, 289 (2015).
- [24] M. Brodt, T. Han, N. Dale, E. Niangar, R. Wycisk, and P. Pintauro, *J. Electrochem. Soc.*, **162**, 84 (2015).

- [25] B. Martinez-Vazquez, D. G. Sanchez, J. L. Castillo, K. A. Friedrich, and P. L. Garcia-Ybarra, *Int. J. Hydrog. Energy*, **40**, 5384 (2015).
- [26] S. Martin, B. Martinez-Vazquez, P. L. Garcia-Ybarra, and J. L. Castillo, *J. Power Sources*, **229**, 179 (2013).
- [27] K. Tang and A. Gomez, *J. Colloid Interface Sci.*, **184**, 500 (1996).
- [28] S. Martin, P. L. Garcia-Ybarra, and J. L. Castillo, *J. Power Sources*, **195**, 2443 (2010).
- [29] J. Zeleny, *Phys. Rev.*, **10**, 1 (1917).
- [30] G. Taylor, *Proc. R. Soc. Math. Phys. Eng. Sci.*, **280**, 383 (1964)
- [31] K. Hiraooka, in *Fundamentals of Mass Spectrometry*, K. Hiraooka, editor, Vol. 8, p.145, Springer, New York (2013).
- [32] A. M. Chaparro, B. Gallardo, M. A. Folgado, A. J. Martin, and L. Daza, *Catalysis Today*, **143**, 237 (2009).
- [33] R. Benitez, J. Soler, and L. Daza, *J. Power Sources*, **151**, 108 (2005).
- [34] S. Martin, P. L. Garcia-Ybarra, and J. L. Castillo, *Int. J. Hydrog. Energy*, **35**, 10446 (2010).

Chapter 2

Mode Variation of the ES Method with Pt/GCB or Pt/Ta-SnO₂

2.1 Introduction

Many researchers have investigated the basic study about the phenomenon of the ES method [1,2]. Zeleny reported that the preparation forms of droplets were affected by the electric field around the nozzle [3]. Taylor theoretically proved that the meniscus of the nozzle tip becomes a cone when a liquid with an electric conductor is subjected to an electric field, so this is called a Taylor cone today [4].

The electric fields are affected depending on several factors, such as nozzle inner diameter, applied voltage and distance between nozzle and substance (d). In principle, the ES method relies on charging the ink in order to disperse the droplets by electrostatic repulsion, so the conductivity of the ink also affects the form of the Taylor cone. In addition, a high viscosity of the ink is suitable, because the ink has difficulty in flowing from the nozzle due to gravity. These conditions can differ according to from the ink components.

Here, the conditions of the Taylor cone using the inks with Pt/GCB and cation-doped metal oxides Pt/Ta-SnO₂ were investigated.

2.2 Experimental

2.2.1 Preparation of the catalyst ink with Pt/GCB

A Pt catalyst supported on graphitized carbon black (Pt/GCB, TEC10EA30E, Pt loading percentage 29 wt%, Tanaka Kikinzoku Kogyo K. K.) was mixed with Nafion binder (DE521, E. I. Du Pont de

Nemours & Co., Inc.) and solvent (2-propanol:high purity water = 1:1 (vol. ratio)) by use of a planetary ball mill (270 rpm, 30 min, P-6, Fritsch GmbH) and was pulverized by use of a wet pulverizing/dispersing device (150 MPa, Star Burst Mini, Sugino Machine, Ltd.). The inks were stabilized by rotating them with a mill pot rotator (Ketjenblack S, Nitto Kagaku Co., Ltd.) for more than 12 h. This preparation of the ink was developed for the conditions for the ES based on the ink composition used for the PSS.

2.2.2 Preparation of the catalyst ink with Pt/Ta-SnO₂

The Ta-SnO₂ support was synthesized by use of the flame combustion method, which was described in our earlier work [1, 2]. The Ta dopant content in the support was determined to be 2.5 at% by use of inductively coupled plasma-mass spectroscopy (ICP-MS, 7500CX, Agilent Technologies Co.). The synthesized Ta-SnO₂ support was sintered at 800 °C for 4 h in air in a rotary kiln furnace. The surface areas of the Ta-SnO₂ particles were 25.6 m²g⁻¹, estimated by the Brunauer-Emmett-Teller adsorption method (BET, BELSORP MAX, MicrotracBEL Co.). Pt nanoparticles were loaded on Ta-SnO₂ by use of a colloidal method [2-4]. The Pt/Ta-SnO₂ was heat-treated at 400 °C in N₂ for 2 h and then quenched at room temperature. In addition, the Pt/Ta-SnO₂ was heat-treated at 150 °C in 1 vol% H₂ (balance N₂) for 2 h and then quenched at room temperature. The Pt loading amounts of the Pt/Ta-SnO₂ were estimated by use of ICP-MS. The Pt particle size was estimated to be 5.0 ± 0.7 nm from the TEM images. All of the characterization results correspond to the sample obtained after the 400 °C heat treatment. The Pt/Ta-SnO₂ catalyst had a Pt loading of 17.5 wt%. The Pt/Ta-SnO₂ was mixed with Nafion binder and solvent (2-propanol and ultrahigh purity water, 1:1 (vol. ratio)) by use of a ball mill (270 rpm, 30 min). The

inks were stabilized by first rotating them in a mill pot rotator, at least 2 h and then refrigerating them at least 24 h. Without the pot-mill rotation, the viscosities of the inks were significantly unstable. With the pot-mill rotation, the viscosities of the inks decreased over time, becoming stable after 18 h. With use of both the mill-pot rotation and refrigeration, the viscosity of the ink decreased and became remarkably stable. The stabilized inks were rotated with the mill pot rotator again for at least 1 h and were then dispersed with an ultrasonic homogenizer (UH-50, SMT. Co., Ltd.).

2.2.3 Setting parameters of the ES method

The mode changes of ES method were investigated with nozzle inner diameter of the nozzle, applied voltage and d . The nozzle is positioned above the substrate at a vertical distance 2 and 3 cm, and the distance between the nozzle and extractor electrode plate with a single perforation was maintained at 0.5 cm. The surface substance temperature was maintained at 55 °C.

2.3 Results and discussion

2.3.1 The mode changes of ES method with Pt/GCB

The mode changes are shown in Fig. 2-1a,b,c as a function of applied voltage and nozzle inner diameter every $d = 2.0$ cm, 2.5 cm, 3.0 cm. In particular with $d = 2.0$ cm, the images of the tip of the nozzle are also shown in the images in Fig. 2-1a. The cone-jet mode is shown designated by “o.” (between 3.5 kV and 4.2 kV, with nozzle inner diameter of 250 μm). In the low applied voltage region, below 3.4 kV, with nozzle inner diameter of 250 μm , the tip of the ink emanating from the nozzle had a rounded, droplet shape, without constructing a Taylor cone (designated by “x”). This condition is referred to as the drip mode [5, 6], in which each droplet drops onto the membrane

without atomization. At applied voltages greater than 4.2 kV with nozzle inner diameter of 250 μm , the Taylor cone became unstable, with wobbling of the droplet surface (designated by “ Δ ”). This condition is referred to as the multi-jet mode [7, 8], in which the droplets are dispersed by the electrostatic repulsion and are deposited heterogeneously on the membrane. The electric field (E) of the ink surface at the metal nozzle was estimated as follows:

$$E = K (V / r) \quad (\text{Eq.2-1})$$

$$K = 2 / \ln (2d / r) \text{ (needle electrode)} \quad (\text{Eq.2-2})$$

where V is the potential of the metal nozzle, r is the radius of curvature of the tip, and d is the distance to the counter-electrode (substance). The estimated value of E in our system was on the order of 100 MV m^{-1} , based on the results of Eq. 2-1 and 2-2, which is comparable to that for the generation of the stable Taylor cone (Fig. 2-2) [9]. In the case of constant d , the region of the cone-jet mode expanded with increasing nozzle inner diameter. The reason is able to be explained from Eq. 2-1 and 2-2, namely, K decreases with increasing d . Even if the d or nozzle inner diameter changed, the region of the cone-jet mode was nearly unchanged (about 3.5 kV ~ 4.1 kV).

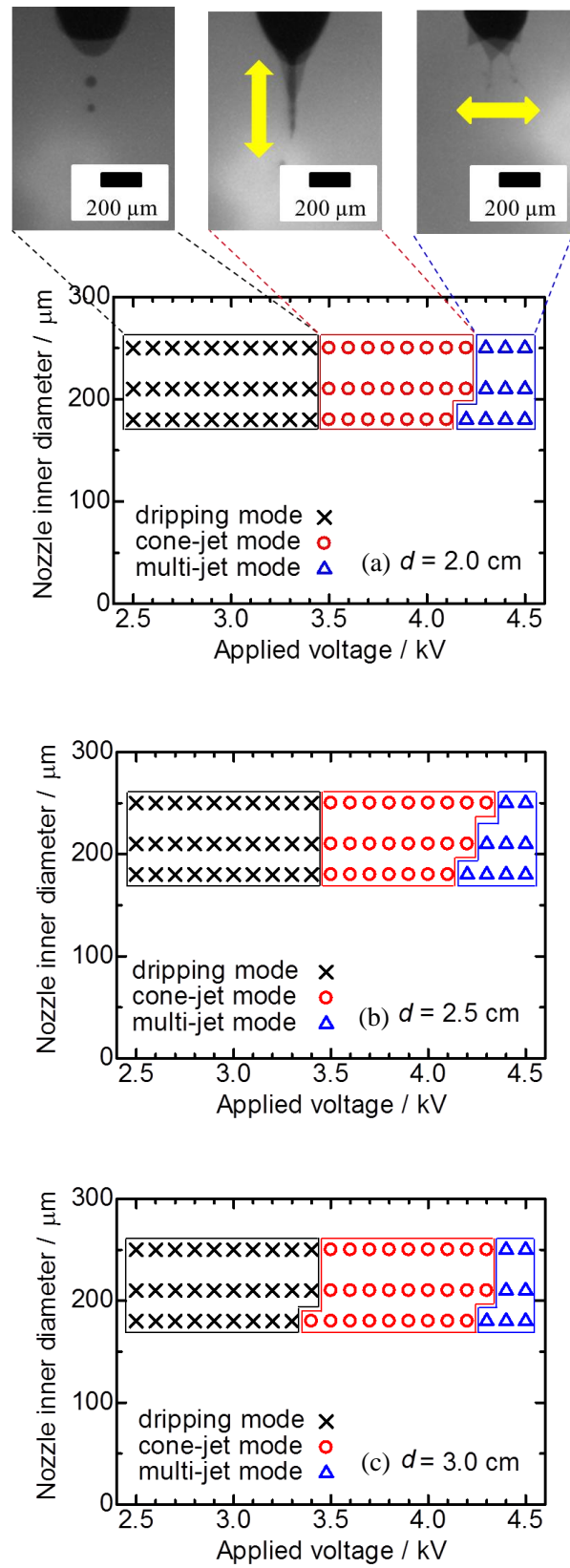


Fig. 2-1 Mode changes with Pt/GCB of Taylor cone as a function of the nozzle-substrate distance and the applied voltage (a) $d = 2.0$ cm, (b) $d = 2.5$ cm, (c) $d = 3.0$ cm.

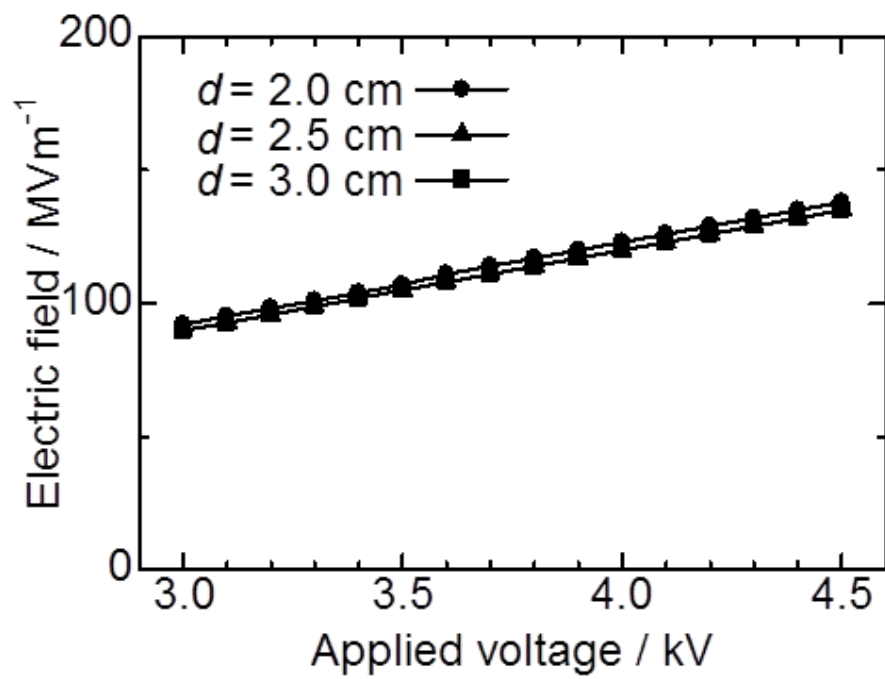


Fig. 2-2 Relationships between the applied voltage and the electric field for various nozzle-substrate distances.

2.3.2 Mode changes of ES method with Pt/Ta-SnO₂

The mode changes of ES method with Pt/Ta-SnO₂ were also measured as in the case of Pt/GCB. However, the viscosity of the ink using Pt/Ta-SnO₂ (5.68 mPa s) was significantly lower than that using Pt/GCB (25.3 mPa s) and thus easily flowed from the nozzle due to gravity. Thus, The ES device was modified Figure 2-3 to control the negative pressure in the ink reservoir between 0.32 kPa (gauge) and 0.38 kPa (gauge) to prevent uncontrolled leakage. The coating modes for the ES method as a function of applied voltage and nozzle inner diameter are shown in Fig. 2-4, a, b, c. As with Pt/GCB, the region of the cone-jet mode expanded with increasing nozzle inner diameter in the case of constant d . Compared with using Pt/GCB, the region of the cone-jet mode with Pt/Ta-SnO₂ was shifted to low applied voltage. The reason can be explained from Eq. 2-1 and 2-2, namely, the E with Pt/Ta-SnO₂ is higher than that with Pt/GCB due to the increase of r . This would be attributed to the difference of the conductivity in the ink.

From these results, the low viscosity ink was able to form the cone-jet mode in the case of controlling the negative pressure in the ink reservoir. The relationship between the viscosity of the ink and the negative pressure in the ink reservoir is shown in Fig. 2-5. This result indicates that the negative pressure in the ink reservoir became high when the viscosity of the ink was low. Therefore, the cone-jet is theoretically able to be formed for low viscosity of the ink.

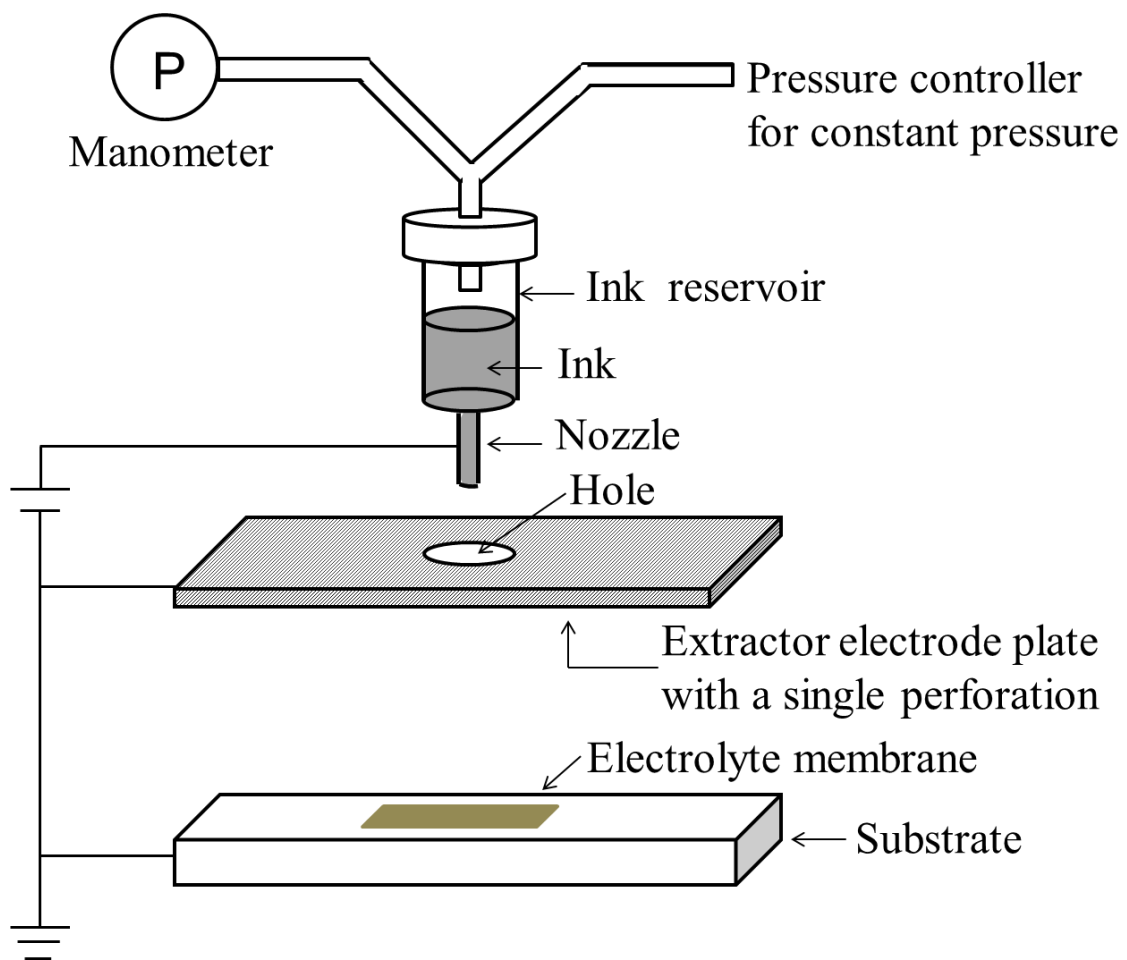


Fig. 2-3 Schematic diagram of the new ES setup and process.

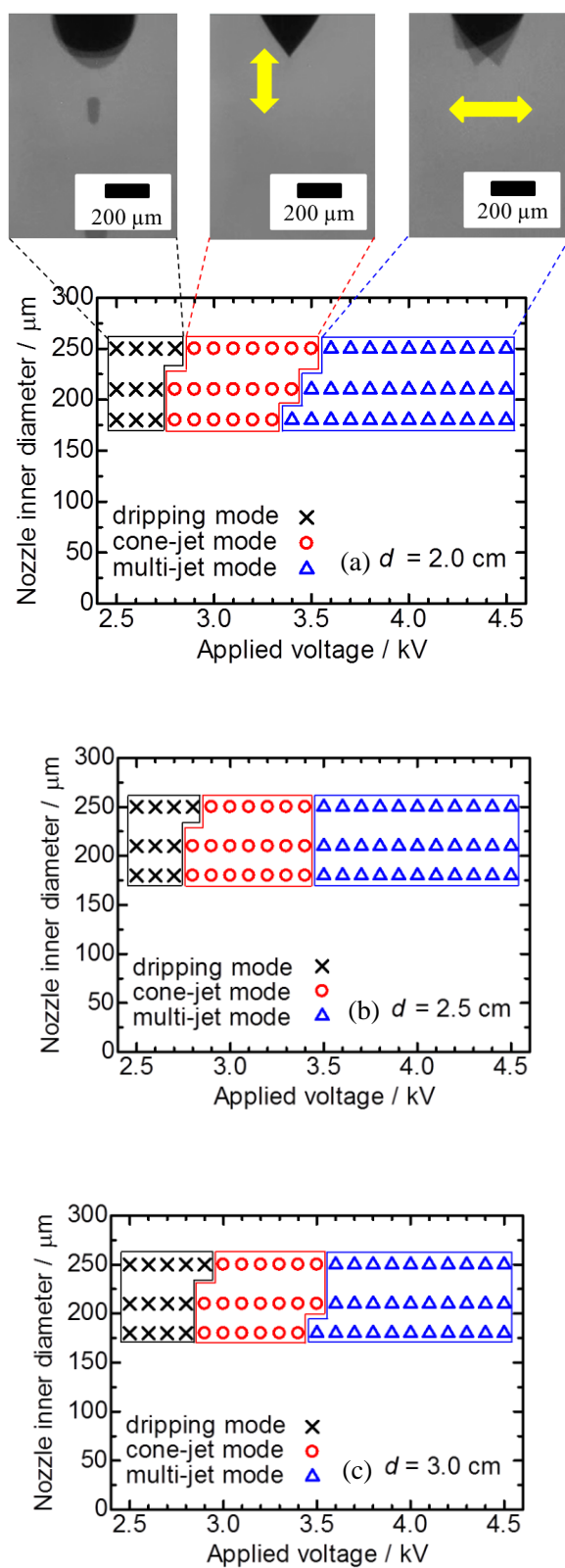


Fig. 2-4 Mode changes with Pt/Ta-SnO₂ of Taylor cone as a function of the nozzle-substrate distance and the applied voltage (a) $d = 2.0 \text{ cm}$, (b) $d = 2.5 \text{ cm}$, (c) $d = 3.0 \text{ cm}$.

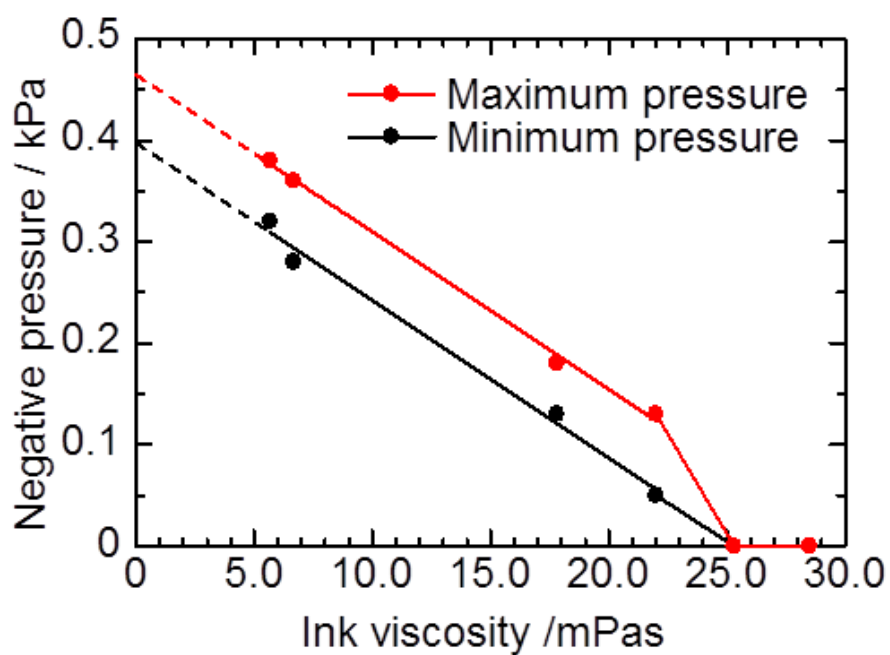


Fig. 2-5 Relationships between the ink viscosity and negative pressure in the ink reservoir.

2.4 Conclusions

Pt/GCB or Pt/Ta-SnO₂ was mixed with Nafion binder and solvent, and the mode changes of ES method were investigated. Both regions of cone-jet mode with Pt/GCB or Pt/Ta-SnO₂ exhibited small differences, and the similar types of behavior were described; the regions of cone-jet mode shifted to high applied voltage with increasing nozzle inner diameter or d . Compared with using Pt/GCB, the region of the cone-jet mode with Pt/Ta-SnO₂ was shifted to low applied voltage. The E values with Pt/Ta-SnO₂ were higher than those with Pt/GCB due to increase of r . This would be attributed to the difference of the conductivity of the ink. In addition, the low viscosity ink was able to form the cone-jet mode in the case of controlling the negative pressure in the ink reservoir. This means that various types of catalyst inks are able to adapt to the ejection with the cone-jet mode of the ES method, even with changes of the catalyst or the mass ratio of binder to support.

2.5 References

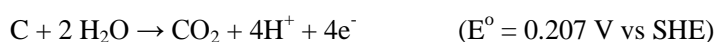
- [1] X. G. Zhang and O. A. Basaran, *J. Fluid Mech.*, **326**, 239, (1996).
- [2] H. Kawamoto, S. Umezumi and R. Koizumi, *J. Imaging Sci. Tech.*, **49**(1), 19, (2005).
- [3] J. Zeleny, *Phys. Rev.*, **10**, 1 (1917)
- [4] G. Taylor, *Proc. R. Soc. Math. Phys. Eng. Sci.*, **280**, 383 (1964).
- [5] E. D. Wilkes, S. D. Phillips and O. A. Basaran, *Phys. Fluids*, **11** (12), 3577 (1999).
- [6] K. Kakinuma, M. Uchida, T. Kamino, H. Uchida, and M. Watanabe, *Electrochimica Acta*, **56**, 2881 (2011).
- [7] K. Kakinuma, Y. Chino, Y. Senoo, M. Uchida, T. Kamino, H. Uchida, S. Deki, and M. Watanabe, *Electrochimica Acta*, **110** 316 (2013).
- [8] M. Watanabe, M. Uchida and S. Motoo, *J. Electroanal. Chem.*, **199**, 311. (1986).
- [9] M. Uchida, Y. Aoyama, M. Tanabe, N. Yamagihara, N. Eda and A. Ohta, *J. Electrochem. Soc.* **142** 2572 (1995).
- [10] M. Cloupeau and B. Prunet-Foch, *J. Electrostatics*, **25**, 165 (1990).
- [11] S. Martin, A. Perea, P. L. Garcia-Ybarra, and J. L. Castillo, *J. Aerosol Sci.*, **46**, 53 (2012).
- [12] J. M. Wilson, *J. Agric. Engng. Res.*, **27**, 355 (1982).
- [13] A. Jaworek and A. T. Sobczyk, *J. Electrostat.*, **66**, 197 (2008).

Chapter 3

Improvement of Cell Performance in Low-Pt-Loading Cathode CLs with Pt/GCB Prepared by the ES method

3.1 Introduction

Platinum-based nanoparticles supported on carbon black (Pt/CB) are typical cathode catalysts for PEFCs [1-3]. The CBs have been adopted as supports for PEFC cathodes because of their high specific surface area, high electrical conductivity and low cost, although the corrosion of the carbon remains a significant issue [4, 5]. Nevertheless, the CBs are attractive support materials for fuel cell vehicle (FCV) and co-generation systems [6], and the cell performance for MEAs prepared by the ES method were reported with Pt/CB [7-9]. However, carbon has an intrinsic thermodynamic instability derived from its oxidative corrosion to carbon dioxide under PEFC cathode conditions. The carbon corrodes seriously when the cathode is exposed to potentials significantly higher than the thermodynamic potential for the following reaction [5, 10].



Carbon corrosion also leads to the isolation of Pt particles from the support surface, deterioration of the cell performance, and thus the cathode performance decreases. [11] As an alternative carbon support to mitigate the carbon corrosion, a graphitized carbon black (GCB) is effective, and beneficial effects have been demonstrated by electrochemical measurements and electron microscopic analysis [12-14]. The information of pore structure and ionomer distribution with Pt/GCB for the ES method is lacking, because no investigations of cell performance with Pt/GCB for the ES method have been reported thus far.

In the chapter, uniform CLs (area 29.2 cm^2) with low Pt loading (0.05 mg cm^{-2}) were prepared by the ES method. The single cell performances were evaluated by use of the standard evaluation cell designed by the Japan Automobile Research Institute (JARI), which is recommended for use as the first step in MEA evaluation by the Fuel Cell Commercialization Conference of Japan (FCCJ). The morphology of the CLs and the performance of the cell were also evaluated, in comparison with that for a CL prepared by the spray method. The attractive features of the ES method were considered.

3.2 Experimental

3.2.1 Preparation of the catalyst ink

Pt catalyst supported on Ketjenblack carbon black (Pt/CB, TEC10E50E, Pt loading percentage 46 wt%, Tanaka Kikinzoku Kogyo K. K.) were applied as the anode. The commercial catalysts were mixed with Nafion binder and solvent (ethanol:high purity water = 2:1 (vol. ratio) by use of a planetary ball mill (270 rpm, 30 min). The preparation method of cathode catalyst inks is described in the previous Chapter (Section 2.2.1, Preparation of the catalyst ink with Pt/GCB).

3.2.2 ES method

The explanations of the mechanism and components for ES method were described in previous chapter (Section 2.2.3 Setting parameters of the ES method). From the results of investigations for the cone-jet mode with Pt/GCB, the capillary nozzle (inner diameter $210 \mu\text{m}$) is equipped with an ink reservoir containing the catalyst ink, and the applied voltage was set 3.9 kV. The nozzle was positioned above the substrate at a vertical distance 2.5 cm, and the distance between the nozzle and extractor electrode plate with a single perforation was maintained at 0.5 cm. The temperature of the

surface of the substrate was maintained at 55 °C. In order to prepare a large-area CL, the substrate stage was able to be moved horizontally at a speed of 15 mm s⁻¹ and to be horizontally shifted with a 0.6-mm pitch. Uniform CLs with an active area of 29.2 cm² were obtained by coating the membrane twice.

3.2.3 Pulse-swirl-spray method

A schematic drawing of the PSS method is shown in Fig. 3-1. In the PSS method (Nordson Co.), the ink is atomized by air with a swirling flow pattern. The ink reservoir was connected to a spray gun, which was equipped with a nozzle (inner diameter 500 μ m). The spray gun was positioned 7 cm above the membrane, which was held by aspiration on a heated porous substrate (surface temperature, 55 °C). The ink was sprayed in a swirl pattern and was atomized on the membrane. The spray gun was horizontally moved at a speed of 50 mm s⁻¹, and the stage of the porous substrate with the membrane was shifted horizontally with a 5-mm pitch. The coating procedure was repeated ten times.

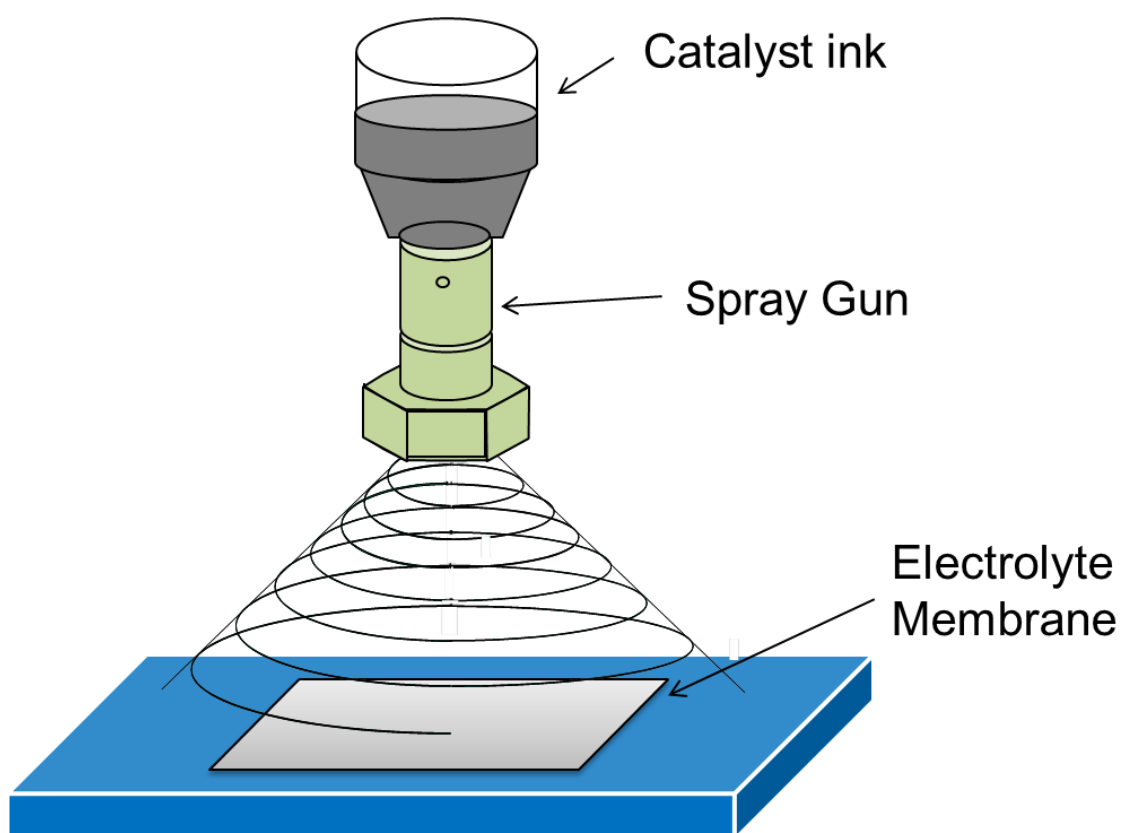


Fig. 3-1 Schematic drawing of pulse-swirl-spray (PSS) method process.

3.2.3 Preparation and evaluation of the CLs fabricated by PSS or ES methods

The anode catalyst ink was prepared by the PSS method on the electrolyte membrane, and the cathode catalyst ink was prepared by either the ES or the PSS method. Each of the CL-coated membranes (CCMs) obtained were dried in an electric oven (60 °C, 12 h), sandwiched by gas diffusion layers (GDLs, 25BCH, SGL Carbon Group), and hot-pressed (140 °C, 10 kgf cm⁻², 3 min.). The Pt loading amounts of these membrane-electrode assemblies (MEAs) were estimated by use of ICP-MS. The Pt loading amounts of the cathode CLs were confirmed to be 0.048 mg cm⁻² (PSS) and 0.056 mg cm⁻² (ES), and that of the anode CLs was 0.50 ± 0.02 g cm⁻². The high Pt loading at the anode was prepared so that there would be negligible anode polarization under all of the experimental conditions. The droplets on the membrane of both methods were observed by use of a digital microscope (VHX-1000, Keyence Co.). Scanning electron microscopic images (SEM) of the catalyst layers were obtained in the SEM mode with a scanning transmission electron microscope (STEM, HD-2700, Hitachi High-Technologies Co.). Cross-sectional samples were prepared by use of a focused ion beam milling system (FIB, FB-2200, Hitachi High-Technologies Co.). The average thicknesses of the CLs were estimated from the values measured at 120 positions on the CL. The occupation fractions of pores in the CLs, based on binarization of the SEM images with high and low magnification, were estimated with an image analysis system (LUZEX-AP, Nireco Co.). The distributions of the ionomer coated on the Pt and GCB support particle surfaces were observed by use of a TEM (HT7700S, Hitachi High-Technologies Co.), with which it was possible to observe the sample with low acceleration voltage (80 kV); this microscope was also equipped with a special high resolution objective lens. This equipment makes it possible to observe soft organic ionomers and inorganic carbon materials at high resolution and high contrast with minimal beam damage [15].

3.2.4 Evaluation of fuel cell performances

Cyclic voltammograms (CVs) of each cathode CL were measured with a potentiostat (HZ-5000, Hokuto Denko Co.) during H₂ flow to the anode (100 mL min⁻¹) and a static N₂ atmosphere at the cathode, both at ambient pressure. Prior to the sweep, the cathodic potential was maintained at 0.075 V for 3.0 s. Then, the potential was swept from 0.075 V to 1.000 V at 20 mV s⁻¹ and reversed back to 0.075 V. The electrochemically active surface areas (ECAs) of each Pt catalysts in the CLs were evaluated from the hydrogen adsorption charge of the CVs, based on a standard value of charge per unit area (Q_H of 0.21 mC cm⁻²) at 30% relative humidity (RH), 53% RH, 80% RH, and 100% RH at 80 °C. The current-voltage (*I-V*) characteristics were evaluated under steady-state operation, after 5 min at each point. The polarization curves were measured in the current control mode. This mode is more common for the evaluation of cell performance of large size MEAs. The cell potential was controlled galvanostatically by use of an electronic load (PLZ-664WA, Kikusui Electronics Co., Ltd.) and was measured as a function of current density by use of a cell performance evaluation-system (FCE-1, Panasonic Production Technology Co., Ltd.). The cell resistance (at 1 kHz) was measured under load by use of a digital ac milliohmeter (Model 3566, Tsuruga Electric Co., Ltd.). H₂ was flowed to the anode and O₂/air to the cathode, and the flow rates of all gases were controlled by use of mass flow controllers. The utilization of reactant gases was 70% for H₂ and 40% for O₂/air. These gases were humidified at 30%, 53%, 80% and 100% RH at 80 °C under ambient pressure (100 kPa).

3.3 Result and discussion

3.3.1 Construction of CLs

Photographs of the areas coated by the PSS and ES methods are shown in Figs. 3-2(a) and 3-2(b). The white dotted line indicates the size of the CL (29.2 cm^2). The areas coated by PSS and ES method were 85.2 cm^2 and 33.6 cm^2 , respectively. Thus, the masked outer area for the PSS method was 56.0 cm^2 , which was approximately twice as large as the geometric electrode area. The masked outer area for the ES method was only 4.4 cm^2 , which was lower by a factor of approximately 13 compared with that for the PSS method. Clearly, the ES method makes it possible to precisely control the coated area and to reduce the loss of the ink. Optical micrographs were obtained of the droplets produced with the of PSS and ES methods on the membrane by use of a digital microscope, as shown in Figs. 3-2(c) and 3-2(d). The average droplet sizes for the PSS and ES method were $82.7 \pm 13.3 \mu \text{ m}$ and $2.35 \pm 0.92 \mu \text{ m}$, respectively. The average droplet size for the ES method was much smaller than that for the PSS method from these photographs. The droplet shapes also differed significantly and indicated that the PSS droplets were wet, while the ES droplets were dry. Specifically, the droplets produced by the PSS method were of nonuniform shape and consisted of catalyst particles in various amounts, because these particles were wet with solvent when they were deposited on the membrane and coalesced during the evaporation of the solvent. In contrast, the droplets produced by the ES method were of uniform shape, because coalescence was prevented due to the low volume of solvent. Even if a more dilute ink was used for the PSS method, the catalyst particles would also coalesce when the wet droplets dried.

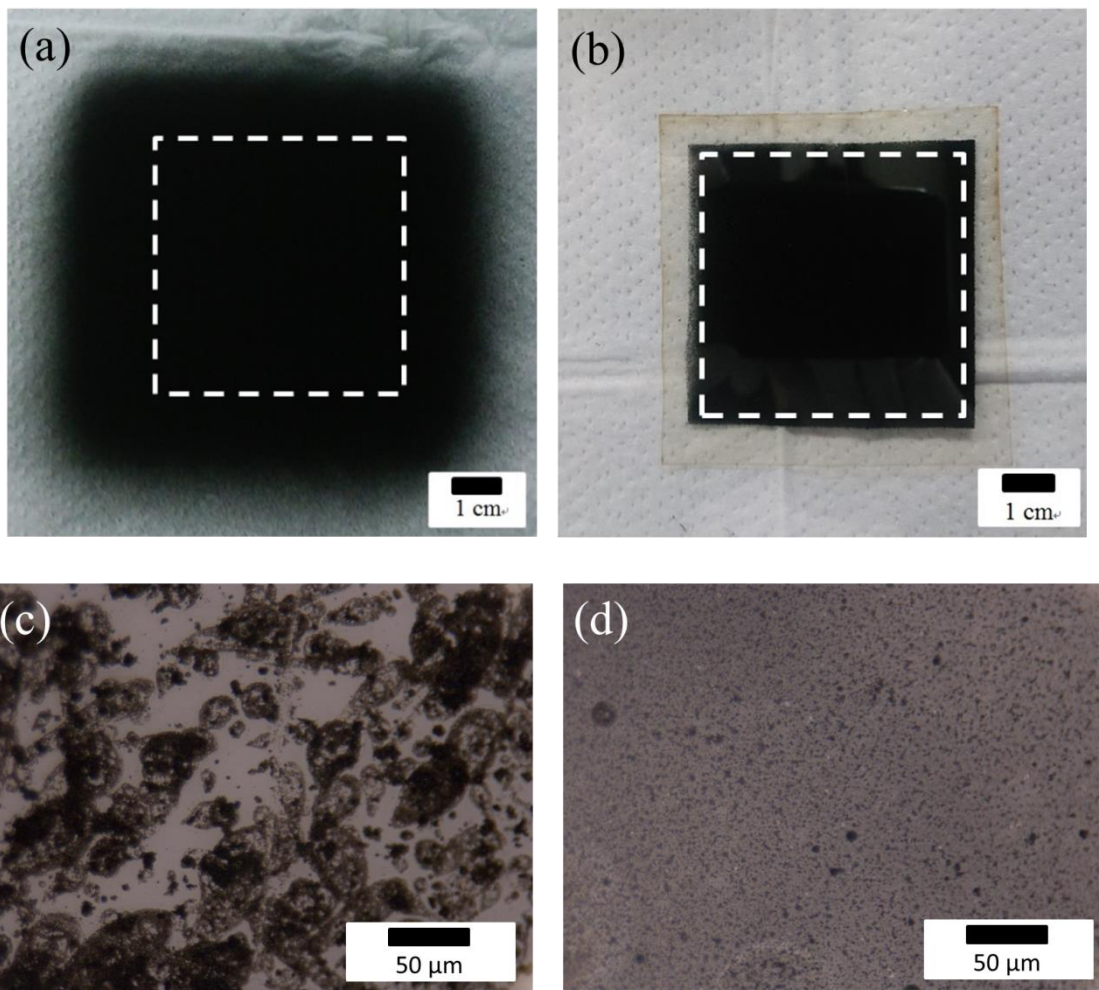


Fig. 3-2 Photographs of CLs on the membrane prepared (a) by PSS method and (b) by ES method. Photographic images of droplets on the membrane prepared (c) by the PSS method and (d) by ES method.

3.3.2 Microstructure of CLs prepared by PSS and ES methods

Low magnification SEM images of the CLs obtained by the PSS (PSS-CL) and ES (ES-CL) methods are shown in Figs. 3-3a and 3-3b. The average thickness of the ES-CL ($16.2 \pm 5.7 \mu\text{m}$) was approximately 3 times larger than that of the PSS-CL ($5.5 \pm 4.9 \mu\text{m}$), in spite of having the same Pt loading amount. The surface roughness for both methods was nearly the same. The large pores, those over 300 nm in diameter, which were estimated from the equivalent circles by the image analysis apparatus, were dispersed throughout both CLs. The occupation fractions of the pores for each CL are summarized in Table 3-1. In the low magnification SEM images (Figs. 3-3a and Figs. 3-3b), the pore fractions for PSS-CL and ES-CL were nearly the same, 0.22 ± 0.024 and 0.23 ± 0.021 , respectively. The high magnification SEM images of both CLs are shown in Figs. 3-3c and 3-3d, and the corresponding pore parameters are also listed in Table 3-1. The total occupation fraction of the pores based on the high-magnification images for the ES-CL was 0.40 ± 0.044 , which was about twice as large as that for the PSS-CL (0.23 ± 0.024). The pore distribution of the GCB obtained by use of mercury porosimetry is shown in Fig. 3-4. The critical change of the cumulative pore volume at about 20 nm indicates the boundary between the primary and secondary pores of the CL. The primary pores are formed between the aggregates of GCB (secondary particles of GCB) [16-18]. The secondary pores are formed between the Pt/CB agglomerates, which are groups of aggregates. The primary and secondary pore fractions of CLs for PSS and ES methods were also evaluated according to the boundary at 20 nm, in Table 3-1. The fraction of small pores (< 20 nm in diameter) in the high magnification images of the ES-CL was 0.072 ± 0.0069 , which was more than twice as large as that for the PSS-CL (0.031 ± 0.0042). The fraction of large pores (> 20 nm in diameter) in the high magnification images of the ES-CL was 0.33 ± 0.036 , which was more than 1.5 times larger than that

for the PSS-CL (0.20 ± 0.022). These results indicate that a more highly porous CL is able to be fabricated by the ES method than by the PSS method. This increase of the pore volume results from increases in the fractions of both small and large pores due to the small ink droplets formed by the electrostatic repulsion. Therefore, the thickness of the CL obtained with the ES method was much larger than that for the CL obtained with the PSS method.

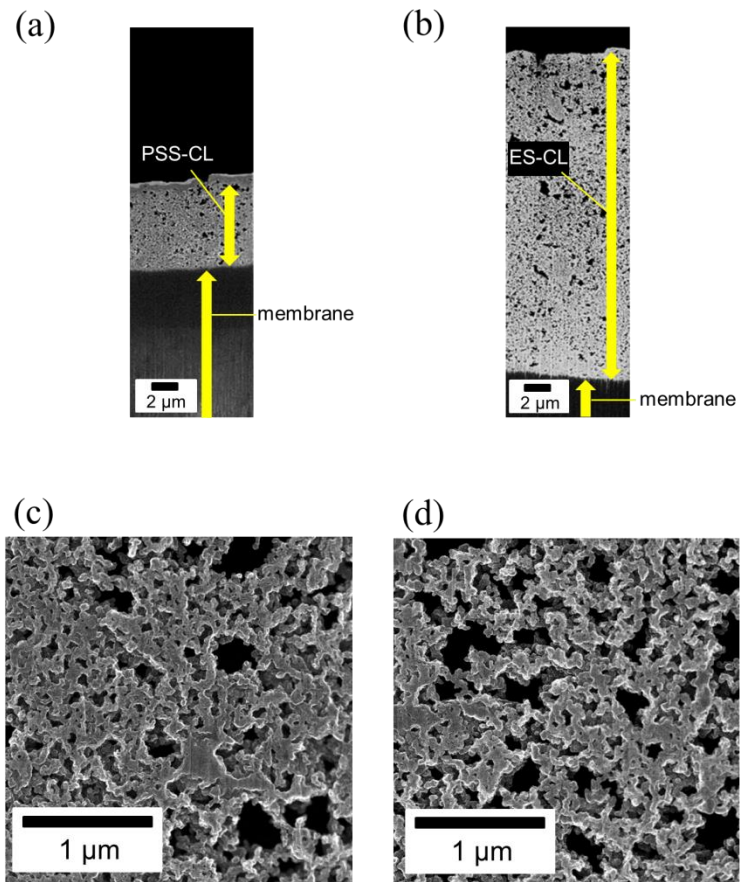


Fig. 3-3 SEM cross-sectional images of cathode CLs prepared (a) by PSS method and (b) by ES method, magnified images of the cathode CLs (c) by PSS method and (d) by ES method.

Table 3-1. Occupation fractions of the pores in the CLs prepared by the PSS and by ES methods in Fig. 3-3, which were estimated from the equivalent circles by use of an image analysis system

Cell	Low magnification images		High magnification images	
	total pore fraction	total pore fraction	primary pore fraction	secondary pore fraction
PSS-cell	0.22 ± 0.024	0.23 ± 0.027	0.031 ± 0.0042	0.20 ± 0.022
ES-cell	0.23 ± 0.021	0.40 ± 0.044	0.072 ± 0.0069	0.33 ± 0.036

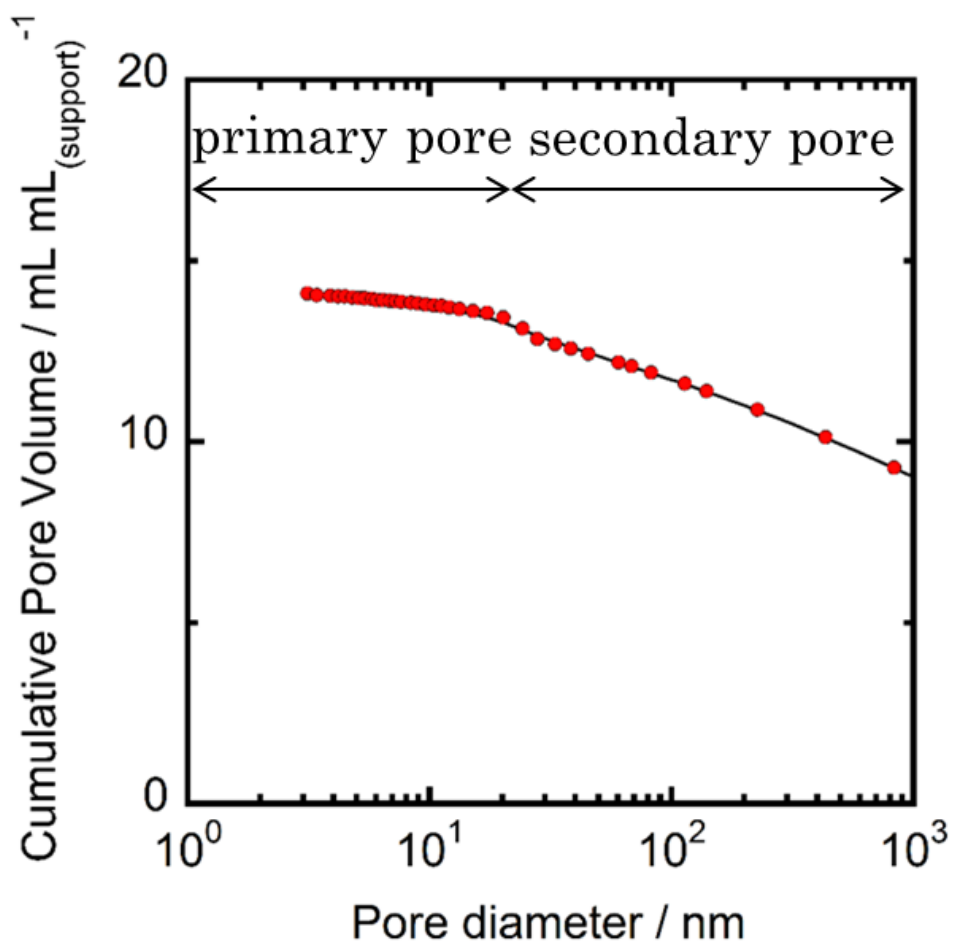


Fig. 3-4 Relationship between cumulative pore volume and pore diameter of the graphitized carbon black.

3.3.3 Performance of the cathodes fabricated by the PSS and ES methods

The CVs for the ES-cell cathode and PSS-cell cathode (80 °C, 100% RH) exhibited the usual hydrogen absorption/desorption peaks and Pt oxidation/reduction peaks (Fig. 3-5a); these peaks were rather similar for the two cathodes. The ECA values, which were determined from the hydrogen adsorption peak for the ES-cell at 80 °C and 30–100% RH, increased 20–10% with increasing humidity and were larger than those for the PSS-cell (Fig. 3-5b). The ECA value at 100% RH at 80 °C was higher than the other values [7]. The ES method makes it possible to effectively construct a porous CL. The increase of the ECA values indicated that the ES method was also effective in improving the ionomer coverage. TEM images are shown in Figs. 3-6a and 3-6b. These images indicate that the ionomer coverage on catalyst particles in a CL prepared using the ES method was clearly larger than that for a CL prepared using the PSS method. The ionomer thickness in the ES CL was approximately 5 nm, and the ionomer was spread uniformly on most of the GCB surfaces. In contrast, the ionomer in the PSS-CL was unevenly distributed. With the ES method, the ink droplets were quite small, in the micrometer range, and thus the drying process during CL fabrication might have been faster than that for the PSS method (Figs. 3-3(c) and 3-3(d)). Such an acceleration of the drying might have an effect on the ionomer coverage.

Fig. 3-7 shows *IR*-free polarization curves for the ES-cell and PSS-cell at 80 °C at 80% RH under O₂/air cathode conditions. The Tafel slopes for the ES-cell and PSS-cell were 84.3 mV decade⁻¹ and 89.5 mV decade⁻¹, respectively, indicating that nearly the same kinetic behavior was occurring for the ORR in both cathode CLs. The cell potential of the ES-cell was higher than that of the PSS-cell for current densities below 0.5 A cm⁻². The dependence of the mass activity (*MA*) on humidity is shown for both cells for the 30–100% RH range in air in Fig. 3-8. The *MA* values for the ES-cell at

0.85 V at each humidity were more than twice as large as those for the PSS-cell. The improvements of the MA for the ES-cell were significantly higher than those for the ECA values (20–10%). These results suggest that the effectiveness of Pt [19] was improved by the use of the ES method, in addition to the improvement of the Pt utilization. Fig. 3-9 shows the current density and ohmic resistance of both cells at 0.70 V under the various RH conditions. The superiority of the performance of the ES-cell compared to that of the PSS-cell decreased with decreasing RH. In order to compare the cell performance to previous cell performance [7-9], Table 3-2 summarizes the current per unit cathode Pt mass at 0.70 V and maximum power for selected evaluation conditions. These data indicate that the performance of our ES cathode is superior to those in previous reports, because the present evaluation conditions included air with zero backpressure. The difference between the ohmic resistances of both cells increased with decreasing RH. The ionomer coverage was clearly improved by the use of the ES method in spite of the ionomer contents of both cells being nearly the same (Figs. 3-6a and 3-6b). The average ionomer thickness on the Pt/GCB surface using the ES method is estimated to be smaller than that using the PSS method. Therefore, the performance superiority of the ES-cell should decrease with decreasing RH, because the ionic resistance of the ES-cell increased more rapidly with decreasing RH than that for the PSS-cell. The high ohmic resistance of the ES electrode was caused by the ionic resistance due to the large CL thickness and small ionomer thickness. At high relative humidity, the large CL thickness caused long proton paths in the CL, and the ohmic resistance increased. However, the ionomer distribution in the ES electrode was uniform and continuous, based on the ECA and MA, and the difference in the ohmic resistance was small. At low relative humidity, the small ionomer thickness in the ES electrode was affected more strongly, because the ionomer network was easy to interrupt. The O₂

gains for both cells, which were obtained under pure O₂ and air feed, are shown in Fig. 3-10 as a function of the current density at 80 °C and various RH values. The O₂ gain values for the ES-cell at lower than 0.5 A cm⁻² at 80–100% RH were lower than those for the PSS-cell. This indicates that the gas supply network of the cathode was improved under these conditions. The highly porous CL obtained using the ES method was considered to have contributed to the improvement of the gas mass transport at current densities below 0.5 A cm⁻² for 80–100% RH. However, for higher current densities and lower RH, the superiority of the ES-cell disappeared. The thick CL obtained with the ES method led to losses of mass transport capability for gas or protons in the high current density range and led to low proton conductance under low RH conditions. For the ES-cell, there is still room for further improvements in ionomer content, Pt loading percentage, type of carbon, and other types of support materials.

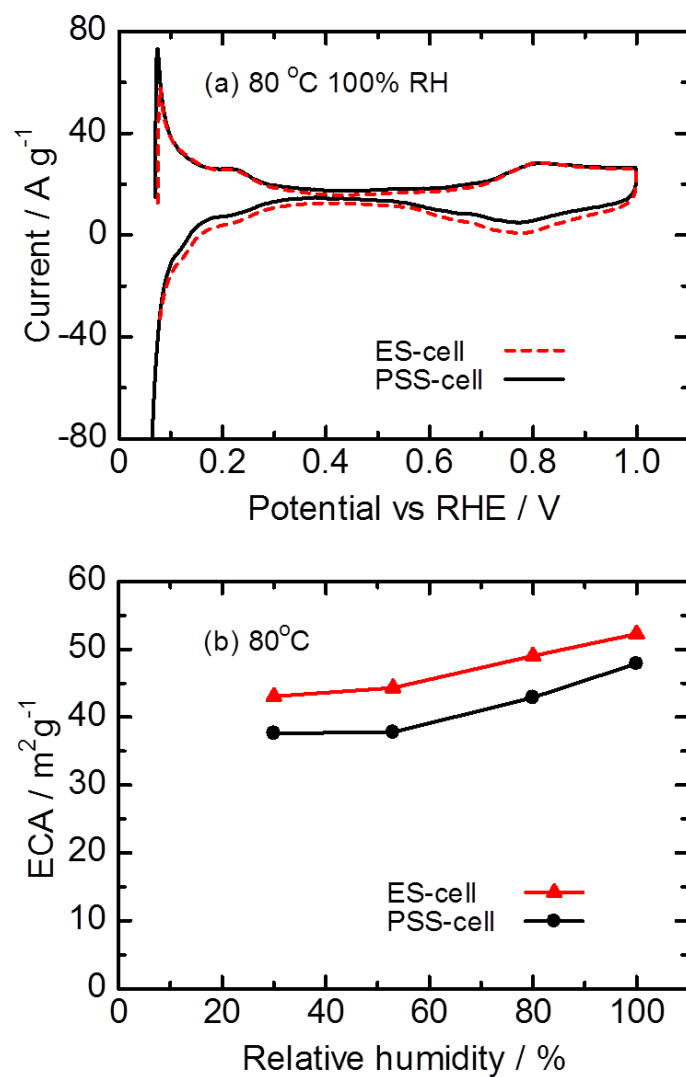


Fig. 3-5 (a) Cathode cyclic voltamograms of ES-cell and PSS-cell at 80 °C, 100% RH, and (b) humidity dependence of the ECA of ES-cell and PSS-cell at 80 °C.

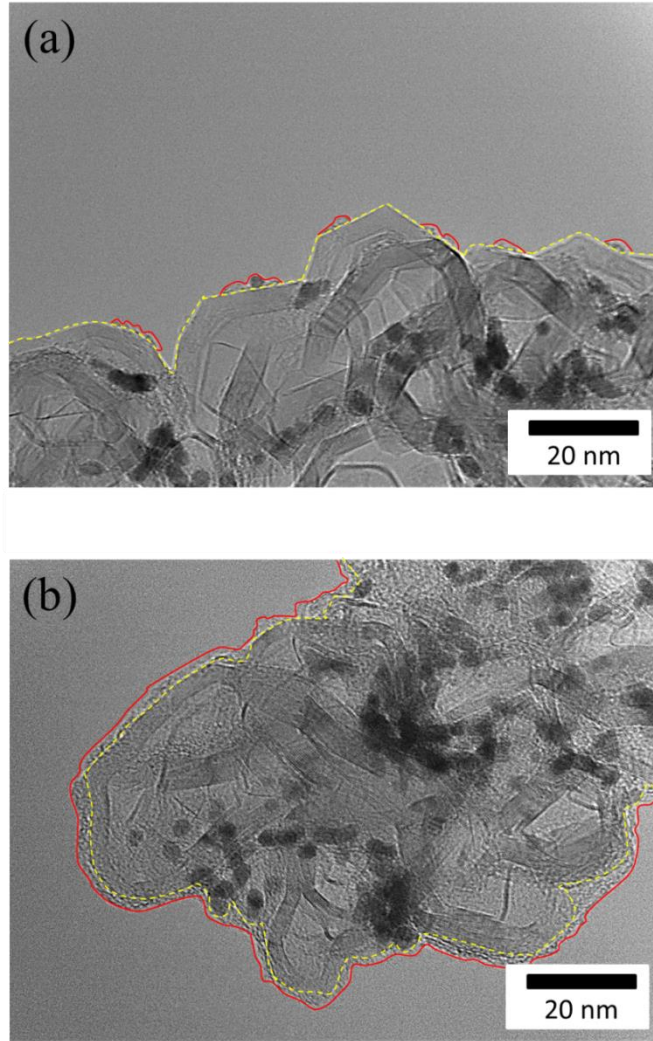


Fig. 3-6 Morphologies of the ionomer covered on carbon-supported Pt catalysts (a) in the PSS electrode and (b) ES electrode.

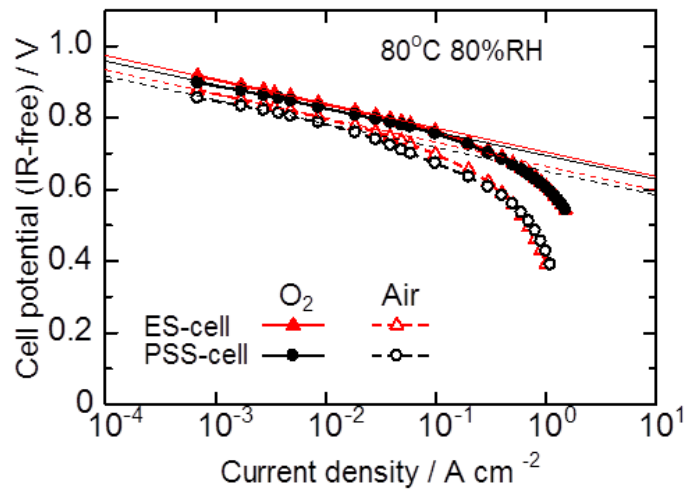


Fig. 3-7 *IR*-free polarization curves for the ES-cell and PSS-cell at 80 °C, 80% RH, air/H₂, ambient pressure.

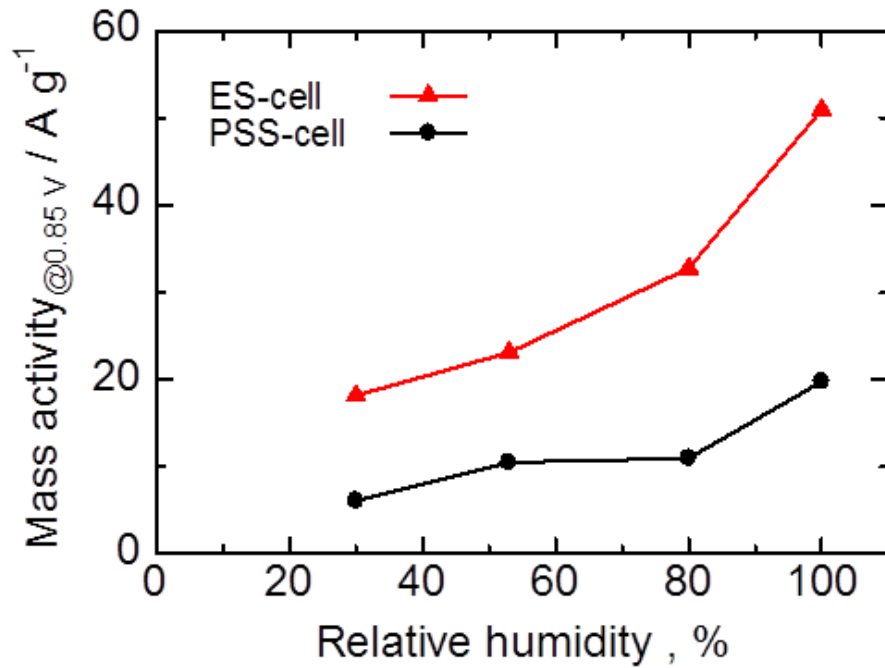


Fig. 3-8 Humidity dependence of mass activity at 0.85 V (*IR*-free), 80 °C, air/H₂, ambient pressure.

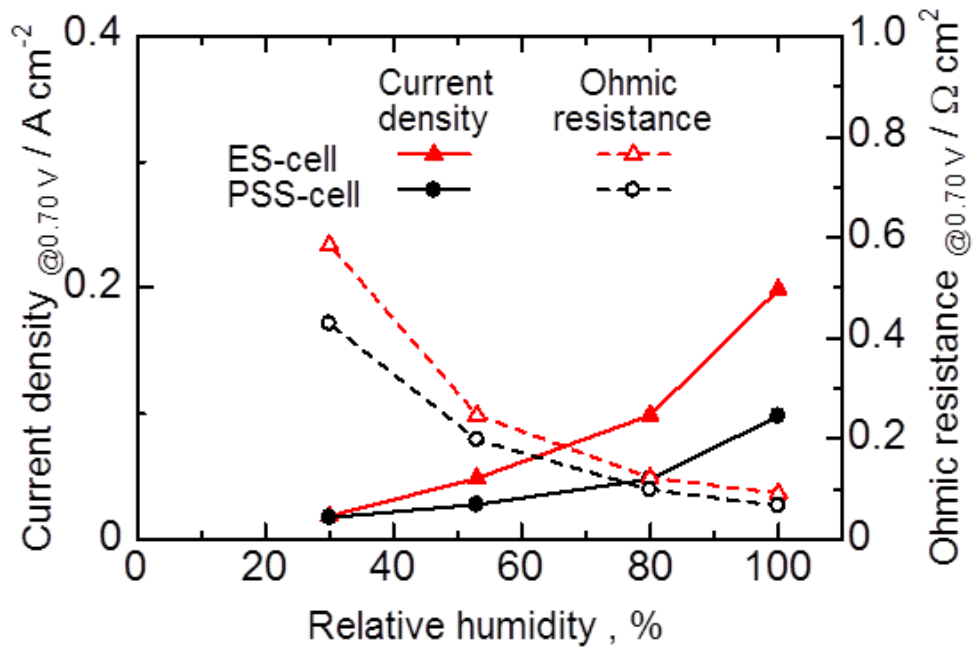


Fig.3-9 Humidity dependence of the current density and the ohmic resistance at 0.7 V (*IR*-free), 80°C, air/H₂, ambient pressure.

Table 3-2 Comparisons of cell performances using various cathode CLs prepared by the ES method

	Pt loading amount / mg cm ⁻²	Electrode size / cm ²	Gas species	Back pressure / kPa	Cell temperature / °C	Gas relative humidity, %	Current per cathode Pt loading amount at 0.7 V / A g ⁻¹	Max power per cathode Pt loading amount / W g ⁻¹
This research ES _{cathode-cell}	0.056	29.2	Air	0	80	100	3546	18222
A. M Chaparro et al., [20]	0.2 0.17	16.0	oxygen	100	80	100	1600 2235	2780 3206
R. Benitez et al., [21]	0.5	9.0	-	0	room temperature	-	289	354
S. Martin et al., [22]	0.012 0.012	-	oxygen	0 340	40 70	0	2083 8333	10400 21000

3.4 Conclusions.

The cathode CLs were prepared by use of the ES method from Pt nanoparticle catalysts supported on GCB and were then evaluated. By optimizing the various preparation conditions, i.e., d , the applied voltage, and the nozzle diameter, etc., the droplets for the ES method were able to maintain a stable ejection of sub-micrometer size, and CLs with highly uniform characteristics were obtained. The ES method enabled us to precisely control the coated area and to reduce the loss of catalyst ink. The ES method also led to improved ionomer coverage, increased ECA values, and more highly porous CLs. The highly porous CL prepared by the ES method contributed to the improvement of the MA and the cell performance due to the increased efficiency of gas mass transport at current densities below 0.5 A cm^{-2} at 80–100% RH. The new method using the ES method for the preparation of thin CLs with very Pt low loading might be attractive in order to improve the performance and reduce costs for PEFCs.

3.5 References

- [1] A. Iiyama, K. Shinohara, S. Iguchi, and A. Daimaru, in Handbook of Fuel Cells, W. Vielstich, H. Yokokawa, and H. A. Gasteiger, Editors, 6 p. 905, John Wiley & Sons, Ltd., West Sussex (2009).
- [2] L. M. Roen, C. H. Paik, and T. D. Jarvi, *Electrochem. Solid-State Lett.*, **7**, 19 (2004).
- [3] T. Yoda, H. Uchida, and M. Watanabe, *Electrochim. Acta*, **52**, 5997 (2007).
- [4] J. P. Meyers and R. M. Darling, *J. Electrochem. Soc.*, **153**, 1432 (2006).
- [5] N. Linse, G. G. Scherer, A. Wokaun, and L. Gubler, *J. Power Sources*, **219**, 240 (2012).
- [6] A. Ohma, K. Shinohara, A. Iiyama, T. Yoshida, and A. Daimaru, *ECS Trans.*, **41**(1), 775 (2011).
- [7] A. M. Chaparro, B. Gallardo, M. A. Folgado, A. J. Martin, and L. Daza, *Catalysis Today*, **143**, 237 (2009).
- [8] R. Benitez, J. Soler, and L. Daza, *J. Power Sources*, **151**, 108 (2005).
- [9] S. Martin, P. L. Garcia-Ybarra, and J. L. Castillo, *Int. J. Hydrog. Energy*, **35**, 10446 (2010).
- [10] H. Tang, Z. Qi, M. Ramani, and J. F. Elter, *J. Power Sources*, **158**, 1306 (2006).
- [11] Y.-C. Park, K. Kakinuma, M. Uchida, H. Uchida, and M. Watanabe, *Electrochim. Acta*, **123**, 84 (2014).
- [12] P. V. Shanahan, L. Xu, C. Liang, M. Waje, S. Dai, and Y. S. Yan, *J. Power Sources*, **185**, 423 (2008).
- [13] C. Wang, M. Waje, X. Wang, J. M. Tang, R. C. Haddon, and Y. S. Yan, *Nano Lett.* **4**, 345 (2004).
- [14] H. Yano, T. Akiyama, P. Bele, H. Uchida, and M. Watanabe, *Phys. Chem. Chem. Phys.*, **12**,

3806 (2010).+

- [15] Y. C. Park, H. Tokiwa, K. Kakinuma, M. Watanabe, and M. Uchida, *J. Power Sources*, **315**, 179 (2016).
- [16] M. Uchida, Y.-C. Park, K. Kakinuma, H. Yano, D. A. Tryk, T. Kamino, H. Uchida, and M. Watanabe, *Phys. Chem. Chem. Phys.*, **15**, 11236 (2013).
- [17] M. Uchida, Y. Fukuoka, Y. Sugawara, N. Eda, and A. Ohta, *J. Electrochem. Soc.*, **143**, 2245 (1996).
- [18] T. Soboleva, X. Zhao, K. Malek, Z. Xie, T. Navessin, and S. Holdcroft, *ACS Appl. Mater. Interfaces*, **2**, 375 (2010).
- [19] M. Lee, M. Uchida, H. Yano, D. A. Tryk, H. Uchida, and M. Watanabe, *Electrochim. Acta.*, **55**, 8504 (2010).

Chapter 4

Improvement of Cell Performance in Low-Pt-Loading Cathode Catalyst Layers with Pt/Ta-SnO₂ Prepared by the ES method

4.1 Introduction

Platinum-based catalysts supported on CB have been adopted as typical cathode catalysts for PEFCs, although these materials undergo degradation under the operating conditions of low pH, high humidity and high potential [1-3], The mechanism were described in detail in the previous Chapter (3.1, Introduction). As alternative supports to carbon, many researchers have focused on metal oxides as cathode catalyst supports. Ioroi reported that Pt supported on Magneli phase Ti₄O₇ and also TiOx were stable at high potentials (<1.5 V), and that a single cell with a 10% Pt/Ti₄O₇ cathode was able to be operated (80°C in 0.67 V with H₂/O₂) successfully for 350 h [4-6]. Other transition metal-based materials such as TiN have also been investigated as carbon-free cathode electrocatalysts for PEFCs [7-13]. We proposed a fabrication method for Sb-doped SnO₂ nanoparticles with CB-like aggregated structures, and reported high durability in the high potential region [14]. In particular, Pt/Ta-doped SnO₂ with CB-like aggregated structures catalyst have high electrical conductivity, and this has been identified as a superior cathode candidate catalyst for PEFCs [15]. Thus, the ES method for the preparation of thin CLs with Pt low loading might be effective in improving the performance and reducing the cost of PEFCs. However, to our knowledge, no investigations of such cell performance have been reported thus far.

In this Chapter, low Pt loading CLs by the ES method with Pt/Ta-SnO₂ are described. This investigation made use of two inks with different mass ratios of Nafion binder to SnO₂ support (I/S).

The cell performances and CL morphology were evaluated.

4.2 Experimental

4.2.1 Preparation of the catalyst ink with Pt/Ta-SnO₂

The synthesis method of Pt/Ta-SnO₂ material and preparation of the catalyst ink with Pt/Ta-SnO₂ were described in in the previous Chapter (Section 2.2.2, Preparation of the catalyst ink with Pt/Ta-SnO₂). The mass ratios of Nafion binder to SnO₂ support (I/S) values were adjusted to 0.2 or 0.7 for the ES method and 0.7 for the PSS method. The catalyst inks were prepared by the ES and the PSS methods for the cathode. The average Pt nanoparticle diameters were estimated from TEM images. The preparation of the anode ink was described in the previous Chapter (3.2.1, Preparation of the catalyst ink).

4.2.2 Preparation of CLs by the pulse-swirl-spray and ES methods

The explanations of the mechanism and components for the ES method were described in Chapter 2 (Section 2.3.2, Mode changes of ES method with Pt/Ta-SnO₂). In order to investigate the cone-jet mode with Pt/Ta-SnO₂, the capillary nozzle (inner diameter 210 μm) was equipped with an ink reservoir containing the catalyst ink, and the applied voltage set to 3.2 kV. The pressure in the ink reservoir was controlled between -0.32 and -0.38 kPa (gauge). The nozzle was positioned above the substrate at a vertical distance 2.5 cm, and the distance between the nozzle and extractor electrode plate with a single perforation was maintained at 0.5 cm. The surface temperature of the substrate was maintained at 55 °C. The PSS method conditions were similar to those describe in the previous Chapter. (Section 3.2.3, Pulse-swirl-spray method). The Pt loading amount were confirmed to be

0.048 mg cm⁻² (PSS I/S = 0.7), 0.048 mg cm⁻² (ES I/S = 0.7) and 0.054 mg cm⁻² (ES I/S = 0.2) by ICP-MS. The droplets deposited on the membrane by both methods were observed by use of a digital microscope. The average thicknesses of these CLs were estimated from the values measured at 100 positions on the CL from scanning electron microscopic mode images of STEM. The anode ink was directly sprayed onto the GDLs by use of the PSS method. The Pt loading amounts of the anode CLs were confirmed to be 0.50 mg cm⁻². The gas diffusion layers (GDLs) had very rough surfaces. A cathode with a low Pt loading would have been adversely affected by the roughness of the GDL surface if the thin CL had been sprayed directly onto it. On the other hand, the anode CL was able to moderate the effect of the roughness of the GDL surface due to the thicker CL. These CCMs were sandwiched between GDEs and GDLs, and hot-pressed (140 °C, 10 kgf cm⁻², 3 min). Cross-sectional samples were prepared by use of FIB. Images of the CLs were obtained in the SEM mode with the STEM described above. The occupation fractions of pores in the CLs, based on binarization of the SEM images with high and low magnification, were estimated with an image analysis system. The distributions of the ionomer coated on the Pt and carbon support particles surface were observed by use of TEM [16]. These CLs with ES and PSS I/S = 0.7 were observed by use of FIB-SEM (Helios NanoLab G3UC, Thermo Fisher Scientific Inc.). Samples for imaging were prepared by attaching small squares (1.0 cm × 1.0 cm) of coated sample on standard aluminum SEM stubs with conductive carbon adhesive. The samples were placed in the vacuum chamber of the FIB-SEM under SEM imaging conditions, and the FIB intensity was kept as low as possible to prevent potential damage of the layer by the beam. Typical imaging conditions were 1 kV and 50 pA in the scanning electron (SE) mode. The FIB acceleration voltage was 30 kV, and the current was 18 pA for all processes (deposition, rough cutting and polishing) with a 4-nm pitch. Binarization of the

SEM images was carried out by use of in-house software supplied by Panasonic. The 3D images were constructed within a volume of $2.5 \mu\text{m} \times 1.7 \mu\text{m} \times 1.0 \mu\text{m}$ from a total of 250 cross-sections of the binarized SEM images. The pore diameter distributions were analyzed by use of an in-house software package from the 3D images.

4.2.3 Evaluation of the fuel cell performance

Cyclic voltammograms (CV) of the cathodes were measured between 0.075 V ~ 1.0 V at 80 °C, 80% RH, and ambient pressure with a potentiostat (PGST30 Autolab system, Metrohm Autolab B.V.) with H₂ flowing through the anode (100 mL min⁻¹) and a static N₂ atmosphere in the cathode. Prior to the sweep, the cathodic potential was maintained at 0.075 V for 3.0 s at 20 mV s⁻¹. The electrochemically active surface areas (ECA) of the Pt catalysts in the cathode CLs were evaluated from the hydrogen adsorption charge of the CV based on the standard value of charge per unit area. The average Pt particle diameter was 5.0 ± 0.7 nm, and the total surface area was estimated from this value. The fraction of the total Pt surface area (termed Pt utilization, U_{Pt}) that is contacted by the ionomer can also be accessed during the ORR in the CL. As a measure of U_{Pt} in the CL of the MEA, the ECA obtained under inert atmosphere has been employed, as determined from the hydrogen adsorption/desorption charge Q_{H} , and the U_{Pt} .

$$U_{\text{Pt}} = \text{ECA} / S_{\text{Pt,TEM}} \quad (\text{Eq.4-1})$$

where the $S_{\text{Pt,TEM}}$ values are the total surface areas of Pt, which were estimated from the average particle size [17].

The *I-V* polarization curves of the MEAs were obtained under the given conditions in steady-state operation, after 5 min at each point. The cell potential was controlled galvanostatically by use of an

electronic load and was measured as a function of current density by use of a cell performance evaluation-system in the H₂ anode and the O₂ or air cathode at 80 °C under ambient pressure (100 kPa) or 150 kPa and 200 kPa as back-pressure. These gases were humidified at 80% relative humidity (RH) by use of heated water bubblers. Both gas flow rates were 100 mL min⁻¹. Based on our previous AC impedance measurements with a Pt/Ta-SnO₂-cathode cell, the high frequency (HF) ohmic resistance was measured at 10 kHz under load by use of a digital ac milliohmmeter (Model 356E, Tsuruga Electric. Co.).

4.3 Result and discussion

4.3.1 Construction of CLs

The droplets were deposited as shown in Figs. 4-1b and 4-1c when the ink was maintained in the cone-jet mode, compared with those deposited by use of the PSS method (Fig. 4-1a). The average droplet sizes were determined from the impact traces as $109.9 \pm 51.8 \mu\text{m}$ (PSS I/S = 0.7), $4.40 \pm 1.39 \mu\text{m}$ (ES I/S = 0.7) and $3.64 \pm 2.55 \mu\text{m}$ (ES I/S = 0.2), respectively. Clearly, there was only a small difference between the average droplet sizes for the two I/S ratios for the ES method in comparison with that for the PSS method from these photographs. The droplet shapes also differed significantly for the ES and PSS methods, similar to the case of Pt/GCB describe in the previous Chapter (Section 3.3.1, Construction of CLs). The PSS droplets were wet, and the shapes were non-uniform. In contrast, the ES droplets were dry, and the shapes were uniform. Similar differences in droplet shapes were described in the previous Chapter using a Pt catalyst supported on GCB (3.3.1, Construction of CLs).

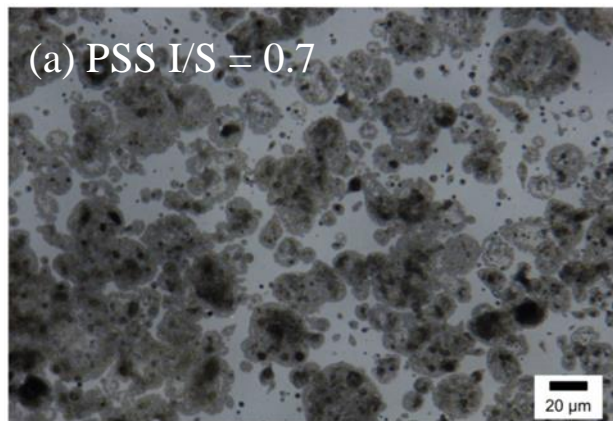


Fig. 4-1 Photographic images of droplets on the membrane prepared (a) by the PSS method with the I/S = 0.7 ink, (b) by the ES method with the I/S = 0.7 ink and (c) by the ES method with the I/S = 0.2 ink.

4.3.2 Morphology comparison of CLs with PSS I/S = 0.7, ES I/S = 0.7 and ES I/S = 0.2

Low magnification FIB-secondary ion microscopy (FIB-SIM) cross-sectional images of PSS I/S = 0.7, ES I/S = 0.7 and ES I/S = 0.2 CLs are shown in Figs. 4-2a, 4-2b and 4-2c. The average thicknesses were $2.1 \pm 1.1 \mu\text{m}$ (PSS I/S = 0.7), $5.4 \pm 0.5 \mu\text{m}$ (ES I/S = 0.7) and $5.8 \pm 0.3 \mu\text{m}$ (ES I/S = 0.2), respectively. The average thicknesses of the CLs for ES I/S = 0.7 and ES I/S = 0.2 were approximately 3 times larger than that for the PSS I/S = 0.7, in spite of having the same Pt loading amount. The droplets produced by the ES method were dry. (Fig. 3b and 3c) Therefore, the droplet morphology would hardly change during hot-pressing. In contrast, the droplets produced by the PSS method were wet. (Fig. 3a) The morphology of the PSS droplets was remarkably changed during drying and hot-pressing. The thickness of CLs prepared by use of the PSS decreased significantly. The large pores ($> 300 \text{ nm}$) were estimated from the equivalent circles by the image analysis apparatus. The occupation fractions of the pores for each CL are summarized in Table 4-1. The pore fractions for CLs with ES I/S = 0.7 (0.33 ± 0.023) and ES I/S = 0.2 (0.36 ± 0.026) were larger than that for the PSS with I/S = 0.7 (0.21 ± 0.024). High magnification SEM cross-sectional images of the CL images are shown in Figs. 4-2d, 4-2e and 4-2f. The extent of small pores (between 20 nm and 300 nm) was also estimated. The occupation fractions of the pores for each CL are also listed in Table 4-1. The pore fractions of CLs with ES I/S = 0.7 (0.42 ± 0.036) and ES I/S = 0.2 (0.45 ± 0.039) were larger than that with PSS I/S = 0.7 (0.25 ± 0.026). Three-dimensional images of the PSS I/S = 0.7 and ES I/S = 0.7 CLs were estimated from the binarized images obtained from the FIB-SEM. The 3-D images are shown in Figs. 4-3a and 4-3b. Both cumulative pore volumes and pore size distributions were calculated from the binarization data (Figs. 4-4a and 4-4b). The cumulative pore volume for ES I/S = 0.7 increased and became significantly larger than that for PSS,

at ca. 40 nm. The porosities of the CLs with PSS I/S = 0.7 and ES I/S = 0.7 were 43.1% and 53.7%, respectively. Thus, even though there were some differences between the results for the various analysis methods, it can be concluded that the ES method was able to produce more highly porous CLs than that for the PSS method.

TEM images are shown in Figs. 4-5a, 4-5b and 4-5c, which indicate the state of ionomer on the catalyst particles in the CLs. The ionomer in the PSS I/S = 0.7 CL was partly disconnected, while the ionomer in the ES I/S = 0.7 and 0.2 CLs was nearly all connected. Magnified images of each electrode show pores between the Pt/Ta-SnO₂ particles (Figs. 4-5d, 4-5e and 4-5f). Large amounts of ionomer filled many of the pores in the PSS I/S = 0.7 and ES I/S = 0.7 CLs. The morphology of the ionomer distribution on the Pt/Ta-SnO₂ catalyst particles that resulted from the ES method hardly changed before/after hot-pressing. This result is in agreement with that for Fig. 4-4a and 4-4b, in which it was shown that the pore volume between 4 ~ 40 μm³ was nearly the same for PSS I/S = 0.7 and ES I/S = 0.7. The difference of pore volumes, with the occupation fractions of the pores for PSS I/S = 0.7 and ES I/S = 0.7, was considered to be due to the advantage of the ES method in forming small ink droplets as a result of electrostatic repulsion. In contrast, the ionomer in the ES I/S = 0.2 CL was thinly coated on the catalyst material, and thus, many pores existed. This explains the fact that the small occupation fraction of the pores in the CL with ES I/S = 0.2 was larger than that with ES I/S = 0.7 (Fig. 4-2 and Table 4-1). The thin, continuous coatings of ionomer obtained by the ES method were considered to have formed due to the droplet size for the ES method being smaller than that for the PSS method (see Fig. 4-1). The average droplet volumes calculated from the droplet impact traces were 695 μm³ (PSS I/S = 0.7), 44.0 μm³ (ES I/S = 0.7) and 25.2 μm³ (ES I/S = 0.2), respectively. The practical droplet volumes would be smaller than those estimated directly from the

impact traces. The volumes of the droplets produced by the ES method were much smaller, one sixteenth ($ES\ I/S = 0.7$) and one twenty-eighth ($ES\ I/S = 0.2$), compared with that produced by the PSS method, based on the images in Fig. 4-1. The very small droplets produced by the ES method can dry quickly, so that the ionomer particles would be directly adsorbed on the surface of the catalyst before the impact on the membrane. Therefore, ionomer coagulation would be impeded, and thin, continuous ionomer coating would be favored.

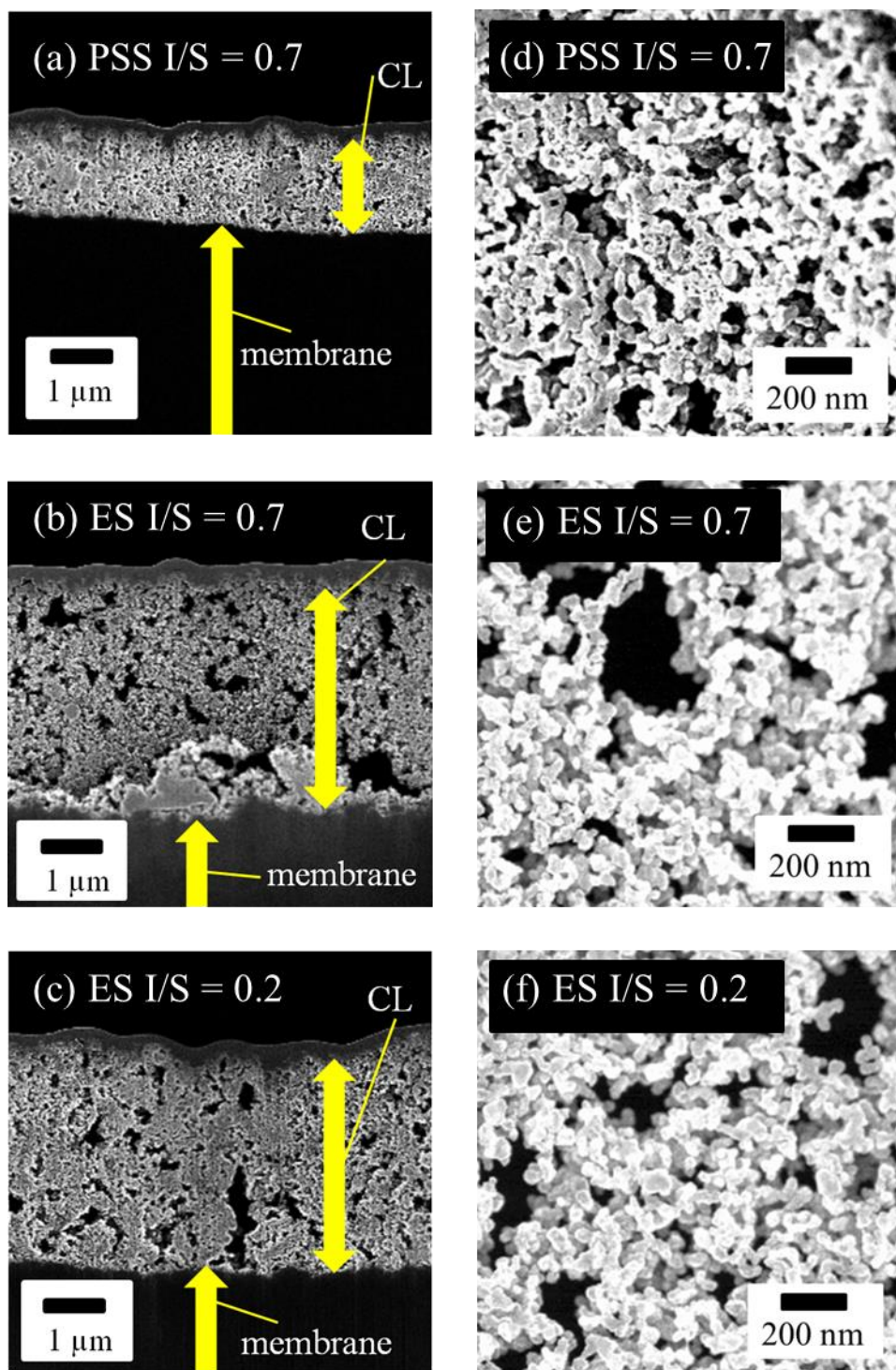
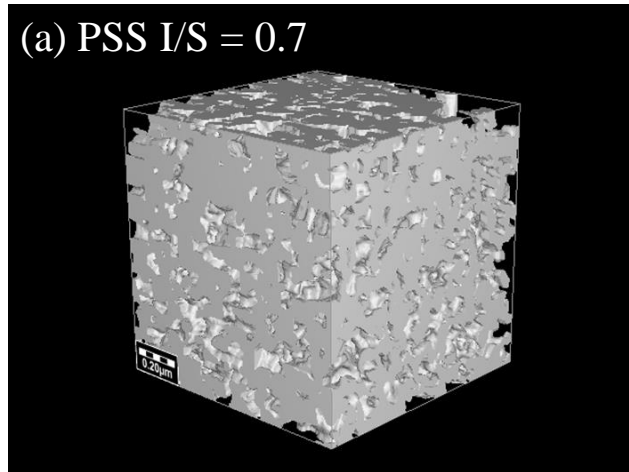


Fig. 4-2 SEM cross-sectional images of cathode CLs prepared (a) by the PSS method with the I/S = 0.7 ink, (b) by the ES method with the I/S = 0.7 ink and (c) by the ES method with the I/S = 0.2 ink, magnified images of each of the cathode CLs shown at left (d), (e), (f).

Table 4-1. Comparisons of pore ratios measured from binarized FIB-SIM images and FIB-SEM.

Cell	Low magnification images	High magnification images	Three-dimensional images
	total pore fraction	total pore fraction	porosity , %
PSS I/S = 0.7	0.21 ± 0.024	0.25 ± 0.026	43.1
ES I/S = 0.7	0.33 ± 0.023	0.42 ± 0.036	53.7
ES I/S = 0.2	0.36 ± 0.026	0.45 ± 0.039	-

(a) PSS I/S = 0.7



(b) ES I/S = 0.7

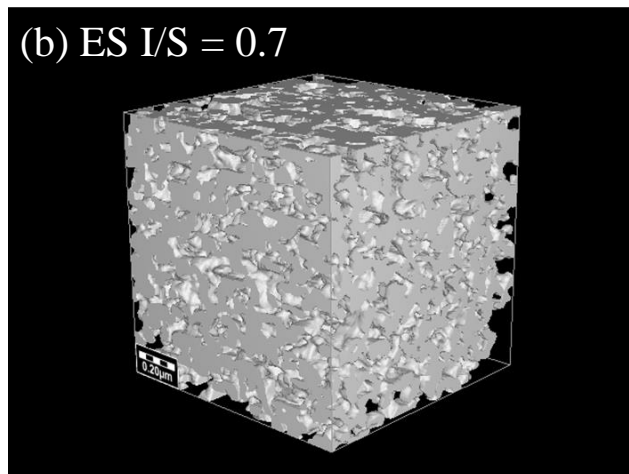


Fig. 4-3 Three-dimensional images (a) of cathode CLs with PSS I/S = 0.7 and (b) of ES I/S = 0.7 estimated based on binarized images obtained from FIB-SEM.

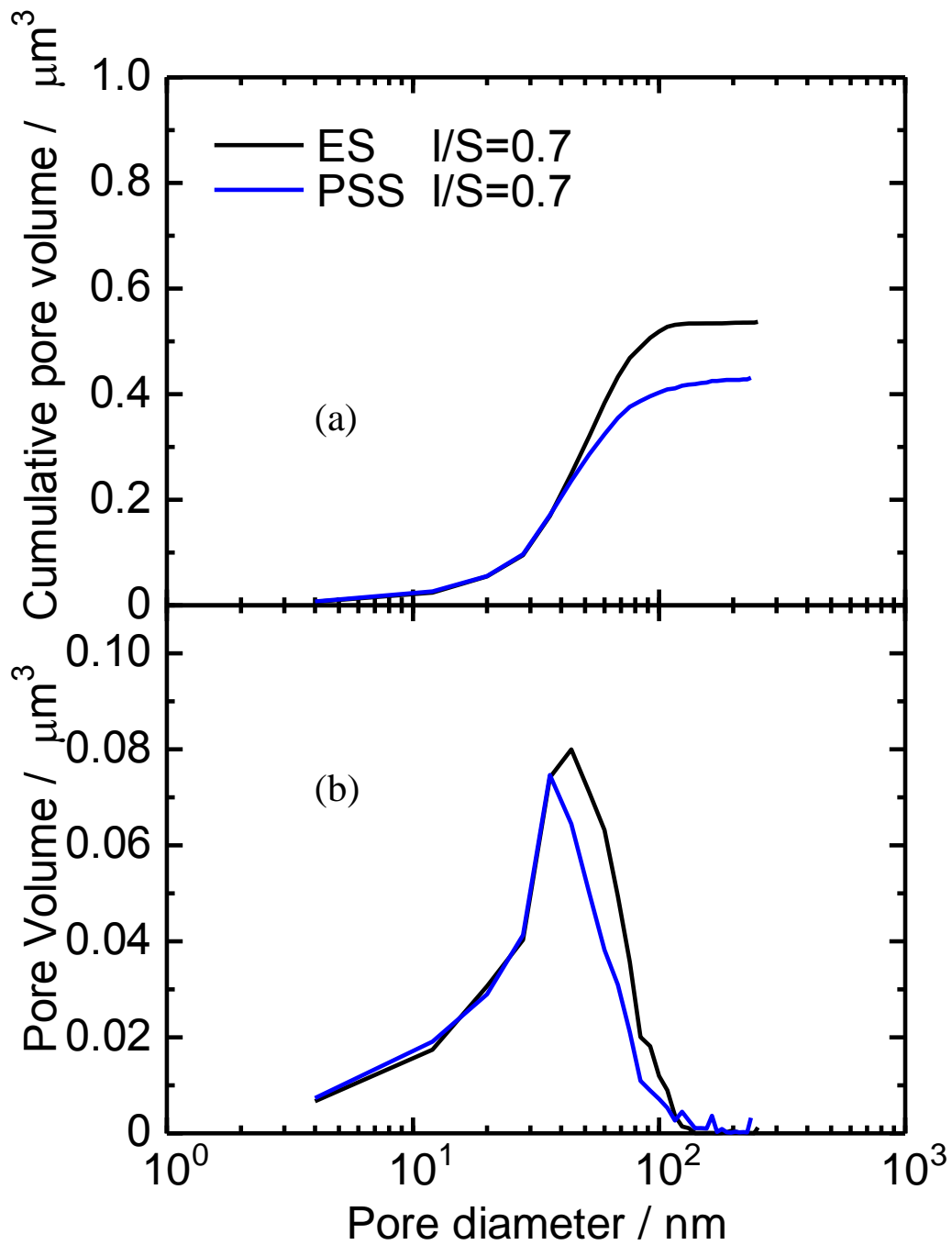


Fig. 4-4 (a) Cumulative pore-volume changes and (b) pore-diameter distributions of pore volume estimated by binarized images obtained from FIB-SEM.

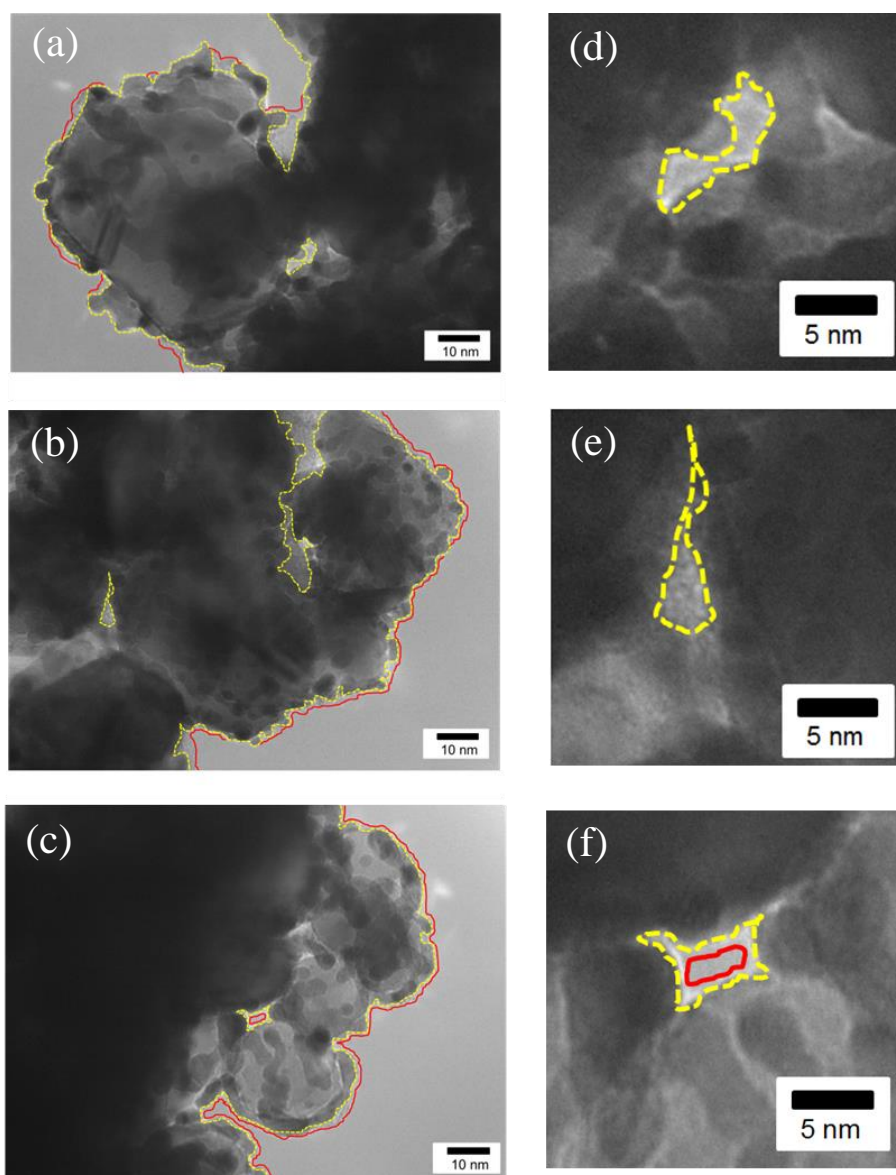


Fig. 4-5 Morphologies of the ionomer covered on Ta-SnO₂-supported Pt catalysts in the (a) PSS I/S = 0.7 electrode, (b) ES I/S = 0.7 and (c) ES I/S = 0.2. Magnified images of the cathode CLs (d), (e), (f) shown at left.

4.3.3 Cell performance comparison of PSS I/S = 0.7, ES I/S = 0.7 and ES I/S = 0.2.

The CV curves (80 °C, 80% RH, ambient pressure) for PSS I/S = 0.7, ES I/S = 0.7 and ES I/S = 0.2 are shown in Fig. 4-6. The CVs exhibited various hydrogen adsorption/desorption charges, and the electrochemically active surface areas (ECAs) were determined from the hydrogen adsorption peak. The ECA values for PSS I/S = 0.7, ES I/S = 0.7 and ES I/S = 0.2 were 43.3 m² g⁻¹, 47.2 m² g⁻¹ and 56.9 m² g⁻¹, respectively. From these ECA and average Pt nanoparticle diameter values, the U_{Pt} values were estimated. The U_{Pt} values for PSS I/S = 0.7, ES I/S = 0.7 and ES I/S = 0.2 were 78.1 %, 85.1 % and 103 %, respectively. The U_{Pt} values for samples obtained with the ES method were larger than that obtained with the PSS method. In particular, the U_{Pt} for ES I/S=0.2 was close to 100%. These results indicate that the ionomer distributions on the Pt particles were remarkably improved with the use of the ES method. The increase of ECA and U_{Pt} indicates that the ES method was effective in improving the ionomer coverage; in particular, for ES I/S = 0.2, the apparent ionomer coverage was high. These results are also consistent with the ionomer distributions shown in Figs. 4-5a, 4-5b and 4-5c.

IR-free polarization curves for all cells are shown in Fig. 4-7a. The cathode measurement conditions were 80 °C at 80% RH under O₂/air (ambient pressure). The performances of the cathodes with CLs produced by the ES method were higher than that using the PSS method for both gases. The ohmic resistances were nearly the same (Fig. 4-7b). The Tafel plots obtained under O₂ and air were also nearly the same (Figs. 4-8a and 4-8b). The mass activities at 0.85 V ($MA_{0.85}$) (Fig. 4-9 and Table 4-2), which indicate the intrinsic activity without mass transport limitations, show that the order of the performance was the same as that for the ECAs values, and the highest value was also obtained for the ES I/S = 0.2 cathode. The $MA_{0.85}$ values for the ES cathodes with I/S = 0.7 and I/S=

0.2 were about twice and three times greater, respectively, than that for the PSS cathode. These results suggest that the effectiveness of Pt was improved by the use of the ES method; in particular, the improvement for ES I/S = 0.2 was remarkable. In the region of low current density, as in the evaluation of mass activity, the cell performance for the lower ionomer content ES cathode was better than that for the higher content. This result can be attributed to the higher ECS for ES I/S = 0.2. We confirmed the uniform coverage of ionomer in Fig. 4-6c. In the region of medium current density, the performance of the ES cathode in air was nearly the same as that for the PSS cathode in O₂, indicating that O₂ diffusion in the CL was significantly improved by the ES method, which is able to form higher porosity CLs (see Figs. 4-2, 4-3, 4-4).

Figs. 4-10a and 4-10b show *IR*-free polarization curves, ohmic resistances and Tafel plots for all cells at 80 °C at 80% RH in air/H₂ with back-pressure, 150 kPa and 200 kPa (absolute). Fig. 4-11 and Table 4-2 show the dependence of mass activity obtained at 0.65 V (*MA*_{0.65}) for all cells. The mass activity at this lower potential includes the effects of mass transport. The cathode performance for ES I/S = 0.7 and 0.2 increased significantly with increasing back-pressure and were eight times greater and ten times greater, respectively, than that for the PSS cathode under both pressure conditions. It was considered that the improvements for the ES I/S = 0.7 and 0.2 CLs were due to both their high porosity and highly continuous ionomer networks, which would facilitate the transport of both O₂ and protons. On the other hand, the voltage at 200 kPa for PSS I/S = 0.7 fluctuated wildly, due to the occurrence of flooding. Therefore, it was not possible to reach higher currents at 200 kPa compared to those for 150 kPa for the PSS method. This result can be attributed to the lower pore volumes of the CLs obtained by use of the PSS method. The ohmic resistances were nearly the same, as were the Tafel slopes, at both back-pressures. In particular, the remarkable

improvement in performance for ES I/S = 0.2 indicates that the ES method is able to construct highly effective transport networks for both O₂ and protons in the CL with low amounts of ionomer. Table 4-3 summarizes the ECA, and the $MA_{0.85}$ and $MA_{0.65}$ values for selected evaluation conditions. Comparison studies used various carbon-supported Pt catalysts. The values evaluated in the present research were superior to those obtained both in our previous research and in other ES research [19], and were comparable with those obtained by use of the electrospinning method [20].

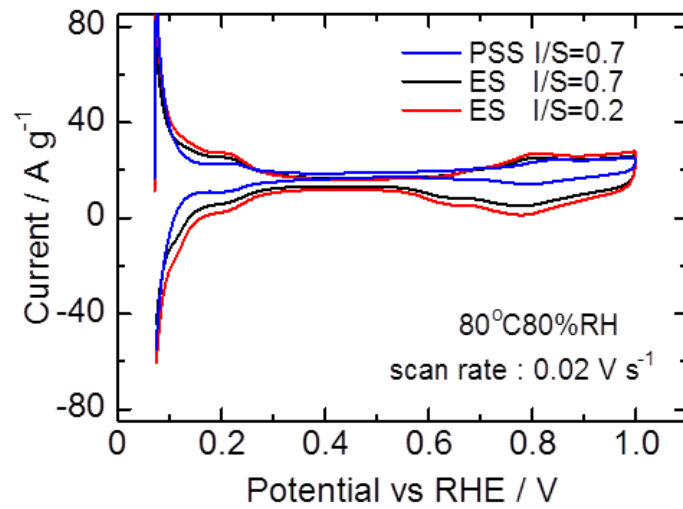


Fig. 4-6 Cathode cyclic voltamograms for PSS I/S = 0.7, ES I/S = 0.7 and ES I/S = 0.2 at 80 °C, 80% RH.

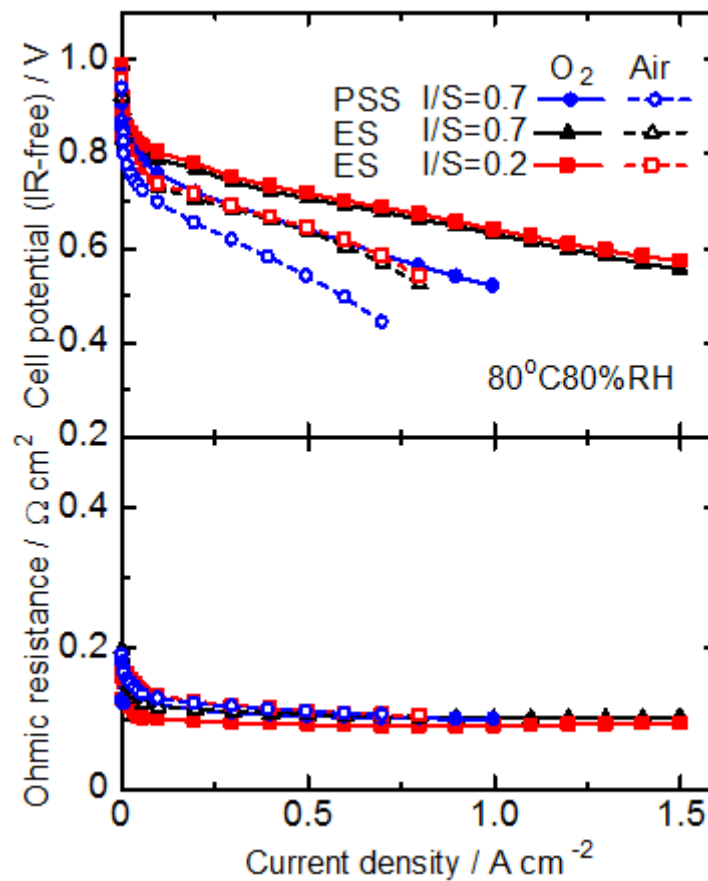


Fig. 4-7 (a) IR-free polarization curves and (b) ohmic resistances for PSS I/S = 0.7, ES I/S = 0.7 and ES I/S = 0.2 at 80 °C, 80% RH, O₂ or air/H₂, ambient pressure.

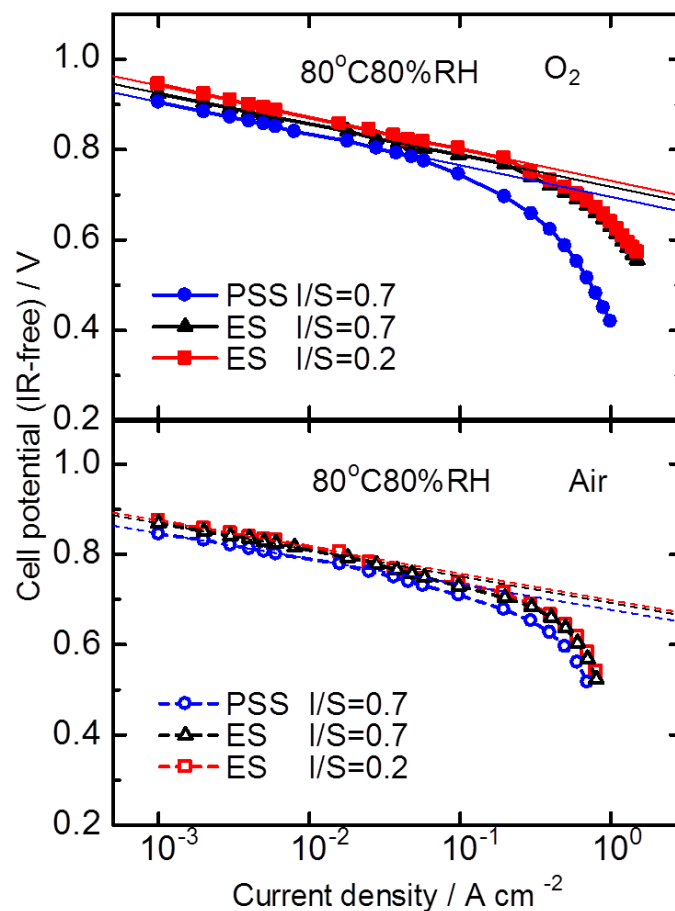


Fig. 4-8 Tafel plot with O₂ (a) or air (b) for PSS I/S = 0.7, ES I/S = 0.7 and ES I/S = 0.2 at 80 °C, 80% RH, O₂ or air/H₂, ambient pressure.

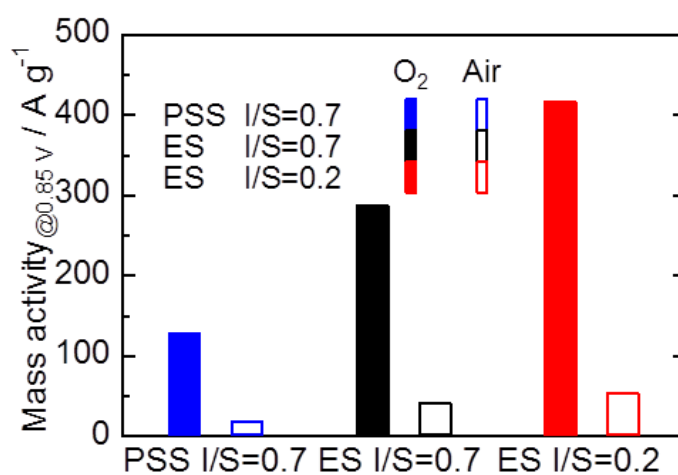


Fig. 4-9 Mass activity at 0.85 V (*IR*-free), for PSS I/S = 0.7, ES I/S = 0.7 and ES I/S = 0.2 at 80 °C, 80% RH, O₂ or air/H₂, ambient pressure.

Table 4-2 Comparisons of cell performances at 80 °C 80% RH using various cathode CLs.

	ECA with	$MA_{0.85}$ with back-pressure 100 kPa		$MA_{0.65}$ in air / $A g^{-1}$		
	back-pressure	(absolute) / $A g^{-1}$		Back-pressure	Back-pressure	Back-pressure
	100 kPa	oxygen	air	(absolute)	(absolute)	(absolute)
	(absolute)			(absolute)	(absolute)	(absolute)
	$/ m^2 g^{-1}$			100 kPa	150 kPa	200 kPa
PSS I/S = 0.7	43.3	129	18.9	411	671	814
ES I/S = 0.7	47.2	287	42.0	3840	5340	6890
ES I/S = 0.2	56.9	416	53.9	6830	7890	9450

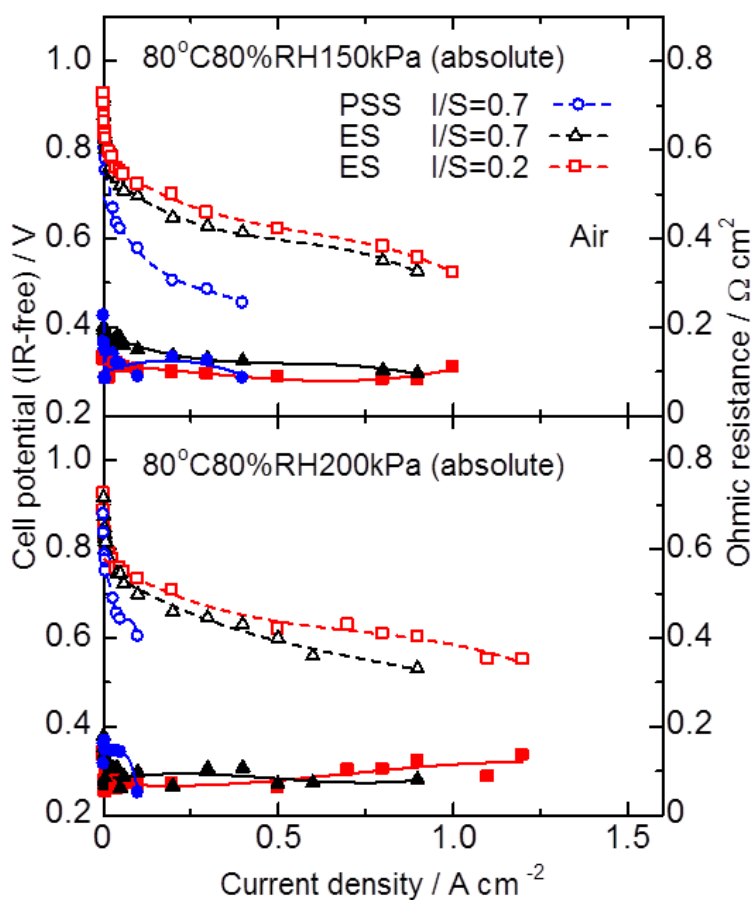


Fig. 4-10 IR-free polarization curves, ohmic resistances for PSS I/S = 0.7, ES I/S = 0.7 and ES I/S = 0.2 at 80 °C, 80% RH, air/H₂, back-pressure 150 kPa (absolute) and 200 kPa (absolute).

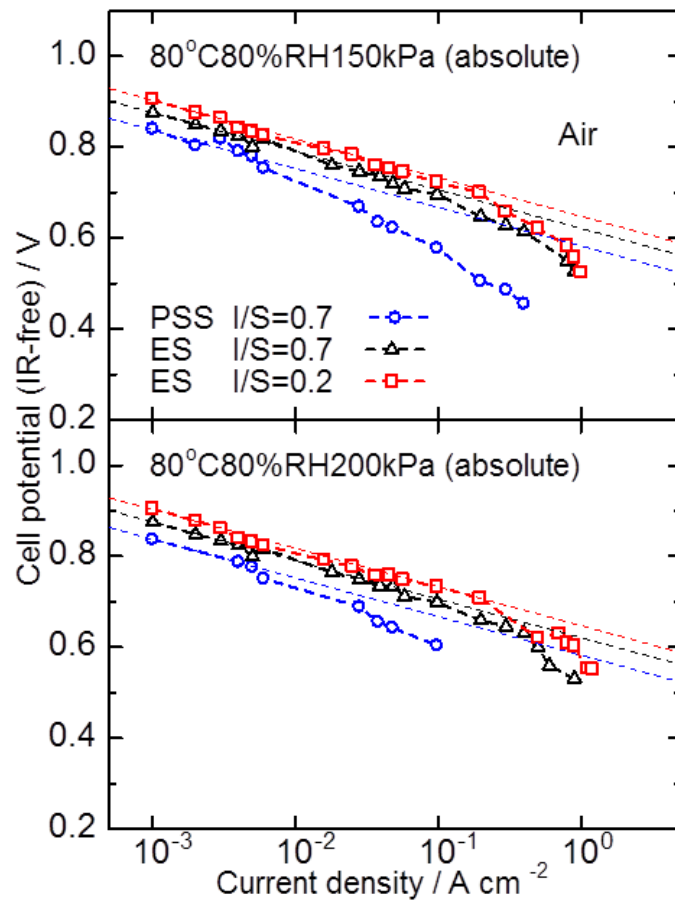


Fig. 4-11 Tafel plots for PSS I/S = 0.7, ES I/S = 0.7 and ES I/S = 0.2 at 80 °C, 80% RH, air/H₂, back-pressure 150 kPa (absolute) and 200 kPa (absolute).

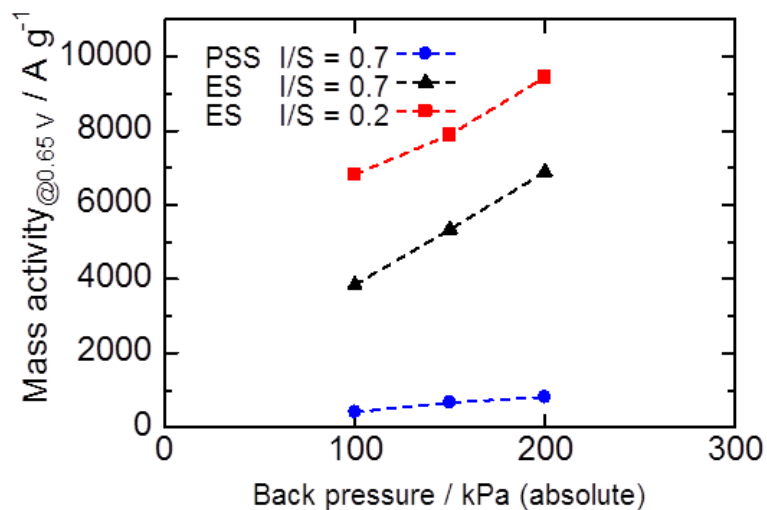


Fig. 4-12 Mass activity at 0.65 V (c) for PSS I/S = 0.7, ES I/S = 0.7 and ES I/S = 0.2 at 80 °C, 80% RH, air/H₂, back-pressure 150 kPa (absolute) and 200 kPa (absolute).

Table 4-3 Comparisons of cell performances using various cathode CLs at 80 °C.

	Support material	Pt loading amount / mg cm ⁻²	Electrode size / cm ²	Gas species	Back-pressure (absolute) / kPa	ECA** / m ² g ⁻¹	Gas relative humidity, %	MA _{0.85} / A g ⁻¹	MA _{0.65} / A g ⁻¹
This research ES-cell	Ta-SnO ₂	0.054	4.4	Air	100	57	80	54	2700
	Ta-SnO ₂	0.054	4.4	Air	200	58	80	65	9500
Previous research ES-cell [18]	Graphited HSAC*	0.056	29	Air	100	50	80	51	3600
A. M. Chaparro et al. ES-cell [19]	Advanced HSAC*	0.25	49	Air	200	43	100	20	2700
P. Pintauro et al., Electrospinning-cell [20]	HSAC*	0.10	5.0	Air	100	-	100	40	7100
	Vulcan	0.10	25	Air	200	64	100	71	9000

* HSAC = high surface area carbon.

** ECAs were evaluated under the conditions of the corresponding research.

4.4 Conclusions

Low Pt loading (0.05 mg cm^{-2}) CLs were prepared by the ES method with Pt/Ta-SnO₂. The characteristics obtained were compared with those for CLs were prepared by the PSS method. The average droplet size for the ES method was approximately one thirtieth of that obtained with the PSS method. The significant decrease of droplet size facilitated the production of highly porous CLs with uniform ionomer covering and improved the cell performance due to the effective transport networks for both O₂ and protons in the CL. In particular, the performance obtained for the ES cathode with low ionomer content ($I/S = 0.2$) was about three times greater for *MA*_{0.85}, and ten times greater for *MA*_{0.65}, than the corresponding values for the PSS cathode.

4.5 References

- [1] T. Yoda, H. Uchida, and M. Watanabe, *Electrochim. Acta*, **52**, 5997 (2007).
- [2] T. Aoki, A. Matsunaga, Y. Ogami, A. Maekawa, S. Mitsushima, K. Ota and H. Nishikawa, *J. Power Sources*, **195**, 2182 (2010).
- [3] H. Yano, T. Akiyama, P. Bele, H. Uchida, and M. Watanabe, *Phys. Chem. Chem. Phys.*, **12**, 3806 (2010).
- [4] T. Ioroi, H. Senoh, S. Yamazaki, Z. Siroma, N. Fujiwara and K. Yasuda, *J. Power Sources*, **155**, 321 (2010).
- [5] T. Ioroi, Z. Siroma, N. Fujiwara, S. Yamazaki and K. Yasuda, *Electrochem. Commun.*, **7**, 183 (2005).
- [6] T. Ioroi, T. Akita, M. Asahi, S. Yamazaki, Z. Siroma, N. Fujiwara and K. Yasuda, *J. Power Sources*, **223**, 183 (2013).
- [7] D.H. Lim, W.J. Lee, N.L. Macy and W.H. Smyrl, *Electrochem. Solid-State Lett.*, **12**, 123 (2009).
- [8] S. Yin, S. Mu, M. Pan and Z. Fu, *J. Power Sources*, **196**, 7931 (2011).
- [9] B. Avasarala and P. Haldar, *Electrochim. Acta*, **55**, 9024 (2010).
- [10] Y. Liu and W.E. Mustain, *J. Amer. Chem. Soc.*, **135**, 530 (2013).
- [11] S. Keerthi, H. Rob, C. Stephen, Y. Siyu and Z. JiuJun, *Electrochim. Acta*, **59**, 538 (2012).
- [12] B. Wickman, M. Wesselmark, C. Lagergren and G. Lindbergh, *Electrochim. Acta*, **56**, 9496 (2011).
- [13] A. Ignaszak, C. Song, W. Zhu, J. Zhang, A. Bauer, R. Baker, V. Neburchilov, S. Ye and S. Campbell, *Electrochim. Acta*, **69**, 397 (2012).

- [14] K. Kakinuma, M. Uchida, T. Kamino, H. Uchida and M. Watanabe, *Electrochim. Acta*, **56**, 2881 (2011).
- [15] Y. Senoo, K. Taniguchi, K. Kakinuma, M. Uchida, H. Uchida, S. Deki and M. Watanabe, *Electrochem. Commun.*, **51**, 37 (2015).
- [16] Y. C. Park, H. Tokiwa, K. Kakinuma, M. Watanabe, and M. Uchida, *J. Power Sources*, **315**, 179 (2016).
- [17] Z. Xia, Q. Wang, M. Eikerling, Z. Liu, *Canad. J. Chem.*, **86** 657 (2008).
- [18] K. Takahashi, K. Kakinuma, and M. Uchida, *J. Electrochem. Soc.*, **163** (10) F1182 (2016).
- [19] A.M. Chaparro, P. Ferreira-Aparicio, M.A. Folgado, E. Brightman, G. Hinds, *J. Power Sources*, **325**, 609 (2016).
- [20] M. Brodt, T. Han, N. Dale, E. Niangar, R. Wycisk, and P. Pintauro, *J. Electrochem. Soc.*, **162**, F84 (2015).

Chapter 5

General conclusion

5.1 Conclusions

In order to improve cell performances with reducing Pt loading amount, the fabrication of the ES method for PEFCs was demonstrated. Some researchers adopted as the fabrication method of the low Pt loading CL by taking this advantage of ES method. However, the fabrication of the low Pt loading CL for ES method has just begun to investigate, and the information of the stable ejecting the ink or the analysis of the morphology concerning cell performance is still lacked. Therefore, in this thesis, cell performance and the morphology for ES method were measured.

In Chapter 1, the fundamental about PEFC, current status of the development, and background of this study were mentioned. In addition, the mechanism of ES method was also described.

In Chapter 2, the coating modes with Pt/GCB and Pt/Ta-SnO₂ for ES method were measured to eject the catalyst ink stably. The relationship are described as a function of applied voltage and nozzle inner diameter every $d = 2.0$ cm, 2.5 cm, 3.0 cm. Both regions of cone-jet mode with Pt/GCB or Pt/Ta-SnO₂ were small differences, the similar behavior were described. The regions of cone-jet mode shifted to high applied voltage with increasing the nozzle inner diameter or d . Compared with using Pt/GCB, the region of the cone-jet mode with Pt/Ta-SnO₂ was shifted to low applied voltage. It would attribute to the difference of the conductivity in the ink. In addition, the ejection of ES method is difficult for the use of the low viscosity ink due to flow easily from the nozzle by gravity. Therefore, the ES device was improved to control the negative pressure in the ink reservoir. The improvement was able to eject the low viscosity ink, experimentally confirmed the relationship

between the negative pressures the ink reservoir and the viscosity ink.

In Chapter 3, a uniform CCM by the ES method with a low Pt loading, $0.05 \text{ mg Pt cm}^{-2}$ was prepared. The ES method makes it possible to control precisely the coating area and reduce the losses of the catalyst ink because of smaller droplets and accurate position control, compared with the PSS method. From the morphology of the CL, the total occupation fraction of the pores in the CLs prepared by the ES method was about twice as large as that for the PSS method. Highly uniform CLs were evaluated by use of a standard evaluation cell (area 29.2 cm^2), and led to increased ECA values and MA at 0.85 V . The effects attributed to improve the ionomer coverage of the CL for ES method, and the improvement was also confirmed from TEM image. The highly porous CLs prepared by the ES method contributed to the improvement of the cell performance.

In chapter 4, the low Pt loading CLs with Pt/Ta-SnO₂ were prepared by the ES method. Two CLs were prepared by the ES method with different mass ratios of ionomer binder to support material (I/S), $I/S = 0.7$ and 0.2 , and are compared to that prepared by the PSS method. Both ES CLs have higher porosity than that for the PSS CL like Pt/GCB, and have improved ionomer coverage and increased ECA area and mass activity at 0.85 V . In particular, that for the ES with $I/S = 0.2$ has high porosity and remarkably increased cell performance. The improvement obtained by use of the ES method can be explained on the basis that the coverage and uniformity of ionomer are increased due to the small droplet size. The performance of the ES cells is high, particularly under high backpressure conditions, because of the improved transport of both O₂ and protons.

From these results, we propose that the new method using ES method for the preparation of thin CLs with low Pt loading might be attractive in order to improve the performance and reduce costs for PEFCs. Our results will help to lay a foundation for new, low Pt loading, high performance PEFC

cathodes.

5.2 Future prospects

From the results of my research and all of relevant research, crucial factors and remained issues which must be solved in achieving higher performance for ES method have been revealed.

(1) Durability test with Pt/GCB and Pt/Ta-SnO₂ for ES method in PEFCs environments

The low Pt loading CL for ES method was shown in high cell performance. The effect attributes to uniform ionomer distribution and highly porous CL, the improvements affect durability test. In particular, Ta-SnO₂ has wide potential ranges with high electrochemical stability in presence of Pt, compared with the others. This advantage of Ta-SnO₂ is able to simplify the single cell operating and reduce the costs of additional systems to control the potential, as a results, the utilization of Pt/Ta-SnO₂ cathode in Fuel cell vehicle can be promoted. This point will be discussed below.

(2) Fabrication of CL for ES method to improve more efficiently cell performance

The analysis of current density distribution during cell performance was shown in ununiformed current density distribution at inlet and outlet or under rib and flow channel. From the results, more efficient CL would be able to achieve by patterned electrodes such as CL depicting the flow channels, it is difficult to fabricate the complex CL because many fabrication devices are not able to control the coating position accurately. However, ES method has potential to solve this problem. Therefore, I would like to fabricate the efficient CL by ES method.

List of publications

“Improvement of Cell Performance in Low-Pt-Loading PEFC Cathode Catalyst Layers Prepared by the Electrospray Method” **Kento Takahashi**, Katsuyoshi Kakinuma, and Makoto Uchida. *J. Electrochem. Soc.*, **163** (10) F1182 (2016)

“Improvement of Cell Performance in Low-Pt-Loading PEFC Cathode Catalyst Layers with Pt/Ta-SnO₂ Prepared by the Electrospray Method” **Kento Takahashi**, Ryo Koda, Katsuyoshi Kakinuma, and Makoto Uchida. *J. Electrochem. Soc.*, **164** (4) F235 (2017)

Meeting abstracts

1. **Kento Takahashi**, Makoto Uchida, Hiroyuki Uchida, Masahiro Watanabe. The 54th Battery symposium in Japan, Oct., 2013, Osaka, Japan,
2. **Kento Takahashi**, Makoto Uchida, Katsuyoshi Kakinuma, Masahiro Watanabe. “Improvement of cathode catalyst layers for PEFCs by the electrostatic inkjet method”, The 3rd International Seminar on Green Energy Conversion, Aug., 2014, Hokuto, Japan,
3. **Kento Takahashi**, Masahiro Watanabe, Makoto Uchida. “Improvement of cathode catalyst layers for PEFCs by the electrostatic inkjet method” The International Chemical Congress of Pacific Basin Societies 2015, Dec., 2015, Honolulu USA,
4. **Kento Takahashi**, Katsuyoshi Kakinuma, Makoto Uchida. “Improvement of cell performance

in low Pt loading cathode catalyst layer prepared by electrospray method for polymer electrolyte fuel cells”, The 5rd International Seminar on Green Energy Conversion, Aug., 2016, Minamisaku, Japan,

5. **Kento Takahashi**, Ryo Koda, Katsuyoshi Kakinuma, Akihiro Iiyama, Makoto Uchida. The Meeting of Electrochemical Society in Japan, Mar., 2017, Machioji, Japan,

Acknowledgements

The present thesis is the summary of work conducted at Research on Nanotechnology for High Performance Fuel Cells and Interdisciplinary Graduate School of Medicine and Engineering University of Yamanashi from 2012 to 21017.

The author would like to express his deepest gratitude to his direct supervisor, Professor Makoto Uchida of University of Yamanashi, for his continuous guidance, invaluable suggestion, and warm encouragement throughout the course of this work.

The author also would like to express his sincere thanks to Professor Katsuyoshi Kakinuma of University of Yamanashi for his helpful suggestion to this work.

The author also would like to express his gratitude to Professor Masahiro Watanabe of University of Yamanashi for his beneficial suggestion to this work.

The author also would like to appreciation to Professor Hiroyuki Uchida of University of Yamanashi for his valuable suggestion to this work.

The author also would like to express his gratitude to Professor Akihiro Iiyama of University of Yamanashi for his valuable suggestions and warm encouragement.

The author is grateful to Professor Donald Alexander Tryk, Professor Kenji Miyatake, Professor Junji Inukai, Professor Tomio Omata, Professor Kazutoshi Higashiyama, Professor Takao Tsueda, Associate Professor Sinji Nohara, Associate Professor Hiroshi Yano, Assistant Professor Masanori Hara, Assistant Professor Youngchul Park, Associate Professor Mitsuru Wakisaka, Assistant Professor Hanako Nishino, Assistant Professor Junpei Miyake, Guest Professor Kenji Kunimatsu, and Guest Professor Hisao University of Yamanashi, for their suggestions and warm encouragement.

I am grateful to Dr. Kazuyuki Tada and Kenji Ikeda of Fuji Xerox Co., Ltd. for helpful advice on the ES method.

I am grateful to Dr. Ryo Koda and Dr. Hiroshi Shintani of Panasonic Corporation for Three-dimensional images of cathode CLs.

I am grateful to Ms. Mika Kodama, Mr. Takahiro Asakawa, Ms. Toshiko Gomyo for the TEM and STEM measurements. I am also grateful to Dr. Takuya Omata, Dr. Masaru Sakamoto, Dr. Satoki Hirakata, Dr. Myoungseok Lee, Dr. Katsuya Nagase, Dr. Yuichi Senoo, Dr. Takayuki Hoshi, Dr. Naoki Yokota, Dr. Haruhiko Shintani, Dr. Ryo Akiyama, Dr. Toshiki Iwataki, Dr. Kriangsak Ketpang, Dr. Morio Chiwata, Dr. Takashi Mochizuki, Dr. Yuji Chino for their helpful advices and valuable discussions.

I would like to thank Mr. Yuki Yamanashita, Mr. Kazuhiro Takanohashi, Mr. Ryo Shimizu, Mr.

Hideaki Ohno, Mr. Haruki Tokiwa, Mr. Yuya Kojima, Mr. Kazuhiro Takanohashi, Mr. Ryonosuke Takei, Ms. Chisato Arata, Mr. Shigefumi Shimada, Mr. Shun Kobayashi, Mr. Naoki Hirayama, Ms. Mizuki Hayashi, Mr. Koki Ueno, Mr. Ryo Kobayashi, Mr. Toshiki Tanaka, Mr. Kanji Otsuji and all of MEA members for their kindly help.

I would like to thank Mr. Yoshiyuki Ogihara, Mr. Hideaki Ono, Ms. Manai Shimada, Mr. Kazuki Shimura, Mr. Masahiro Haraguchi, Mr. Zhang Yaojian, Mr. Ryosuke Nishikawa for their kind support.

I also would like to thank Ms. Toyomi Hayashi, Ms. Kaori Ichinose, Ms. Eri Funato, Ms. Seiko Takano, Ms. Nozomi Toyoda, Ms. Ayako Kobayashi for their kind support.

I would like to thank deeply all members of Fuel cell Nanomaterials Center, Clean Energy Research Center, and Special Doctoral Program for Green Energy Conversion Science and Technology for their kindly help and warm encouragement.

Finally, I would like to thank all of my family for their warm encouragements.

Kento Takahashi

March 2017